Review

Removal of Azo Dyes from Wastewater through Heterogeneous Photocatalysis and Supercritical Water Oxidation

Vincenzo Vaiano [1] and Iolanda De Marco [1,2,*]

1   Department of Industrial Engineering, University of Salerno, Via Giovanni Paolo II, 132,
    84084 Fisciano (Salerno), Italy
2   Research Centre for Biomaterials BIONAM, University of Salerno, Via Giovanni Paolo II, 132,
    84084 Fisciano (Salerno), Italy
*   Correspondence: idemarco@unisa.it

Abstract: Azo dyes are synthetic organic dyes used in the textile, leather, and paper industries. They pose environmental problems due to their toxic and persistent nature. The toxicity is due to the presence of azo groups in the dye molecule that can break down into aromatic amines, which are highly toxic to aquatic organisms and humans. Various treatment methods have been developed to remove azo dyes from wastewater. Conventional wastewater treatments have some drawbacks, such as high operating costs, long processing times, generation of sludge, and the formation of toxic by-products. For these reasons, a valid alternative is constituted by advanced oxidation processes. Good results have been obtained using heterogeneous photocatalysis and supercritical water oxidation. In the former method, a photocatalyst is in contact with wastewater, a suitable light activates the catalyst, and generated reactive oxygen species that react with pollutants through oxidative reactions to their complete mineralization; the latter involves pressurizing and heating wastewater to supercritical conditions in a reactor vessel, adding an oxidizing agent to the supercritical water, and allowing the mixture to react. In this review paper, works in the literature that deal with processing wastewater containing azo dyes through photocatalysts immobilized on macroscopic supports (structured photocatalysts) and the supercritical water oxidation technique have been critically analyzed. In particular, advancement in the formulation of structured photocatalysts for the degradation of azo dyes has been shown, underlying different important features, such as the type of support for the photoactive phase, reactor configuration, and photocatalytic efficiency in terms of dye degradation and photocatalyst stability. In the case of supercritical water oxidation, the main results regarding COD and TOC removal from wastewater containing azo dyes have been reported, taking into account the reactor type, operating pressure, and temperature, as well as the reaction time.

Keywords: heterogeneous photocatalysis; supercritical fluids; textile wastewater; organic pollutants

1. Introduction

Azo dyes are the class of commercial organic dyes most studied due to their wide usage (they represent 70% of the dyes used in the textile industry [1] and are also widely used in the food, cosmetic, and pharmaceutical industries) and their high toxicity. They contain two nitrogen atoms linked by a double bond and two functional groups, R and R'. Their general formula is R–N=N–R', in which one nitrogen atom is hooked up to an aromatic group (R), whereas the other is linked to a substituted aromatic group (R'). The azo bond linkage may be present once (monoazo dyes), twice (diazo dyes), or three times (triazo dyes) [2]. They are typically obtained via diazotization of a primary aromatic amine, followed by coupling with one or more electron-rich nucleophiles, such as amino and hydroxy [3,4]. In general, the chemical structure of an azo dye is represented by a backbone, the auxochrome groups, the chromophoric groups, and the solubilizing groups. The color of azo dye is determined by the azo bonds and their associated chromophores and

auxochromes [5]. As schematically represented in Figure 1, they can be further classified into acid, basic, sulfur, reactive, disperse, and vat dyes.
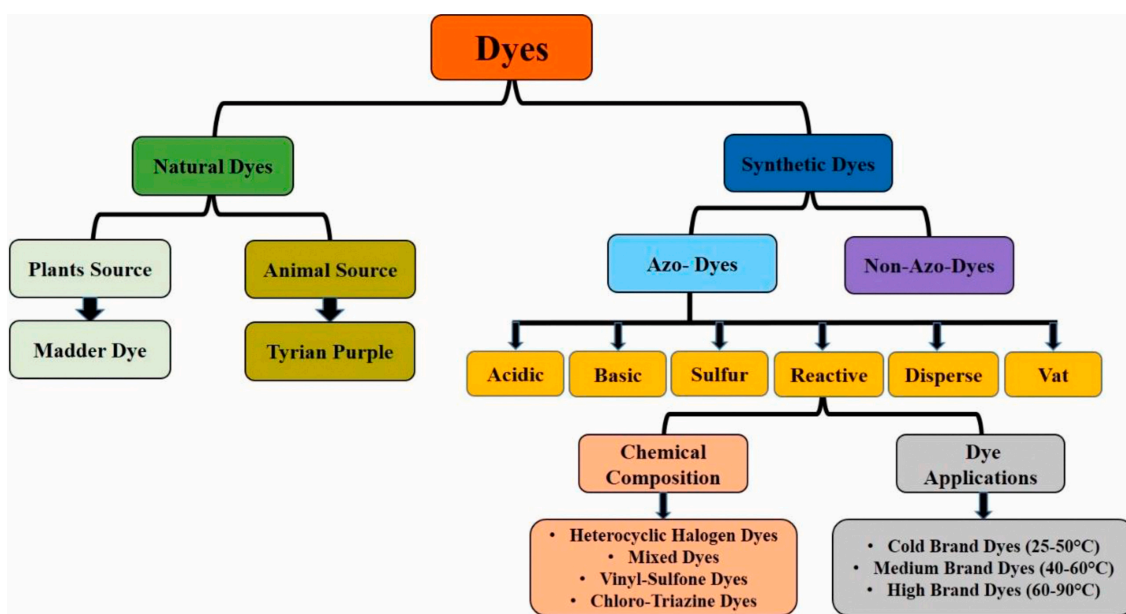

Figure 1. Classification of dyes based on chemical composition and their applications. Reprinted with permission from [6]. Copyright © 2021 Elsevier.

Acid dyes are anionic, water-soluble salts made of sulphonic ($R-SO_3Na$) or carboxylic acid sodium salts ($R-COONa$) that can color wool, nylon, and silk fibers at an acidic pH. **Basic dyes** are cationic salts of organic bases used for dyeing wool, acrylic, and silk fibers. **Sulfur dyes** (amino/nitro aromatic compounds with $-S=S-$ linkages) are the most commonly used in cellulosic textiles for cotton. They are non-ionic and, therefore, insoluble in water; these dyes are predominantly black, brown, and dark blue. **Reactive dyes** are water-soluble anionic dyes constituted of a chromophore, one or two reactive auxophores, and a solubilizing group. They are mainly used for coloring cellulose fibers but can also be applied to wool and nylon. **Disperse dyes** are non-ionic, insoluble, or only slightly soluble in water, synthetic, and typically used on polyester; however, they have also been used on nylon, cellulose acetate, and acrylic fibers. They are polar molecules based on azo compounds; nevertheless, anthraquinone derivatives are frequently used to produce violet and blue colors. **Vat dyes** are insoluble dyes based on anthraquinone or indigo, classified as such because of the method by which they are applied. They are used to color cellulosic materials in a vat.

Several papers in the literature deal with the properties of azo dyes [7–9], evidencing the simplicity in their synthesis procedures, high solubility, and high uptake by the substrate. The properties mentioned above make using azo dyes preferable over other possible organic dyes in textile industries [10]. The extensive use of these dyes by textile industries is the leading cause of environmental pollution problems since they are commonly present in discharged wastewater, releasing potential carcinogenic and toxic substances into the aqueous phase [11,12]. The environmental problem linked to the use of azo dyes is made more severe by the fact that wastewaters from textile industries contain mixtures of dyes with several stable organic components having different structures. The toxic impact of azo dyes is generally due to their high concentration, which confers a strong color on wastewater [7,13].

Consequently, the penetration of visible light into the water is strongly reduced, inhibiting the photosynthesis process [13]. Additionally, because of the aromatic rings in their chemical structure, azo dyes are considered toxic, carcinogenic, and xenobiotic compounds [13–15], which can also cause damage to human beings, including their repro-

ductive and central nervous systems [16]. Figure 2 reports the trend of indexed papers regarding azo dye removal from wastewater. The data were obtained from the Scopus database. The figure shows an exponential trend in the last ten years, underlying the increasing interest of the scientific community in this topic.
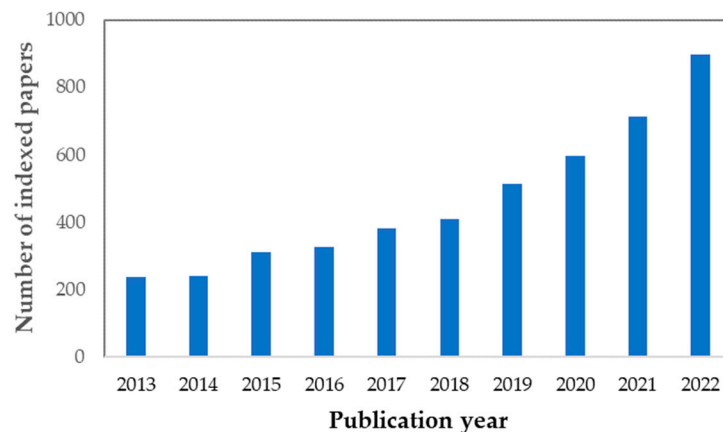

Figure 2. Trend of indexed papers on the topic published in the last ten years. Data taken from Scopus database (using keywords "azo dyes" AND "wastewater").

Considering all such aspects, treatment methods to remove azo dyes through decolorization and detoxification should be performed before discharging textile wastewater into natural water bodies [17,18]. Several physical, chemical, and biological treatments are used for the removal of organic dyes contained in wastewaters, such as coagulation/flocculation [19,20], adsorption [21,22], membrane technology [23,24], and enzymatic degradation [25,26]. Although a high azo dye removal efficiency is achieved using these treatment methods, their main drawback lies in their high operating costs, long processing times, and complicated treatment logistics for large-scale application [27,28]. There are also other disadvantages, such as the generation of sludge, which needs further treatment and makes the process uneconomical, the need to regenerate the adsorbent, and the formation of more toxic by-products [29,30]. Moreover, conventional biological treatments based on bacteria cannot remove azo dyes effectively because of the high chemical stability of synthetic dyes. Moreover, the main disadvantages of the commercial use of chemical oxidation methods, such as electrochemical processes, are their high electrical energy requirements, significant use of chemicals, and the design of proper equipment [31,32]. Moreover, it is worthwhile to underline that conventional biological treatments based on bacteria cannot remove azo dyes effectively because of the high chemical stability of synthetic dyes [14,33].

Therefore, innovative methods for removing azo dyes from water and wastewater must be developed to overcome these drawbacks. From this perspective, advanced oxidation processes (AOPs) could represent an exciting alternative. AOPs are based on generating hydroxyl radicals (OH•) in mild conditions [13,34]. OH• can completely oxidize various water pollutants, including azo dyes [12]. Among the different traditional (i.e., ozonization [35], photo-Fenton [36–39], and UV/H_2O_2 processes [40,41]) and innovative (i.e., non-thermal plasma [42,43] and photoelectrocatalysis [44,45]) AOPs, heterogeneous photocatalysis is still one of the most studied processes for the removal of water pollutants [46] since it can be carried out under UV, visible, or solar light at room temperature and atmospheric pressure using only oxygen as an oxidant, leading to complete mineralization of organic pollutants into CO_2 [47,48]. However, the possibility of generating toxic reaction intermediates during the irradiation time cannot be excluded [31].

Another innovative treatment method is supercritical water oxidation (SCWO) [49]. SCWO, also known as hydrothermal oxidation, consists of the homogeneous oxidation of chemical compounds in an aqueous medium, using oxygen or hydrogen peroxide as the oxidizing agent, at a higher pressure and temperature than water's critical point (i.e., 22.06 MPa and 373.9 °C) [50]. The main application of SCWO is for the destruc-

tion of wastewater and sludges, especially those containing recalcitrant, xenobiotic, and nonbiodegradable pollutants. Compared with AOPs, SCWO technology has several advantages, such as no interphase mass and heat transfer resistance in supercritical water, very high degradation kinetics, and short treatment time (in most cases less than 1 min); indeed, with the appropriate reaction temperature, pressure, and residence time, almost any pollutant can be completely destroyed [50–52]. This process is considered environmentally friendly as it eliminates harmful pollutants, reduces the volume of waste, and produces water and carbon dioxide as the main by-products [53].

Concerning heterogeneous photocatalysis, again, the vast majority of studies in the literature discuss the formulation of powder photocatalysts and testing of their ability to degrade azo dyes in slurry-type photocatalytic reactors [5,54,55]. However, using photocatalysts in powder form requires a further processing step to separate the photocatalyst from the treated water and recover it for reuse [56]. This post-treatment step is a time-consuming and expensive process [57]. To overcome such drawbacks, many efforts have been made to immobilize photocatalysts onto solid macroscopic supports to formulate structured photocatalysts to be used in fixed-bed photoreactors to remove azo dyes [58–60]. However, review papers devoted explicitly to the different structured photocatalysts to be used in the degradation of azo dyes are still scarce. Additionally, to the best of our knowledge, the strengths and weaknesses of SCWO are worth discussing and comparing. For these reasons, the aim of this paper is to provide a comprehensive review of the application of innovative processes based on the use of structured catalysts, such as SCWO and heterogeneous photocatalysis, for the removal of azo dyes in wastewater.

2. Structured Photocatalysts for Azo Dye Removal

2.1. Fundamentals of Heterogeneous Photocatalysis

The mechanism of heterogeneous photocatalysis for the oxidation of organic pollutants is based on the use of semiconductor particles irradiated by light with a suitable amount of energy [61,62]. In detail, when the light energy is greater or equal to the semiconductor band gap, electron–hole ($e-/h+$) pairs are generated [62], and the electrons are promoted from the valence band (VB) to the conduction band (CB) of the semiconductor, causing positive holes in the VB. Positive holes are strongly oxidizing reactive species that can react with H_2O, leading to the formation of OH•. On the other hand, electrons in the semiconductor CB have a strongly reducing power and can react with oxygen dissolved in the liquid medium, generating the superoxide ion (O_{2-}) [61]. Both OH• and O_{2-} can react with organic molecules through oxidative reactions to completely mineralize the target pollutants [63]. Figure 3 reports the simplified mechanism for activating a semiconductor by light.

However, despite the presence of light with the right energy, to achieve high degradation performances, the pollutants must be adsorbed on the photocatalyst surface.

More specifically, the mechanism of heterogeneous photocatalysis (schematized in Figure 4) is based on five main steps: (1) transfer of reactants (A and B) from the liquid phase to the photocatalyst surface; (2) adsorption of the reactants (A * and B *); (3) reaction between the adsorbed reactants, producing the product (AB); (4) desorption of P from the semiconductor surface and (5) transfer of the product into the bulk of the liquid phase [63].

A wide variety of undoped and doped semiconductors, including TiO_2, ZnO, SnO_2, WO_3, Fe_2O_3, and CdS, were studied for the purification of water/wastewater polluted by azo dyes under UV, visible, and solar light thanks to their good photocatalytic performances, light absorption properties, charge carries transport characteristics, and simple preparation process [60,64–72]. However, as pointed out above, most photocatalysts are used as suspended particles in slurry photocatalytic reactors, making separating and recovering these powder photocatalysts necessary after completely removing dyes, limiting the application of a photocatalytic process at the industrial scale. Consequently, photocatalysts should be immobilized within the photoreactor to avoid the post-treatment separation step [61,73,74].
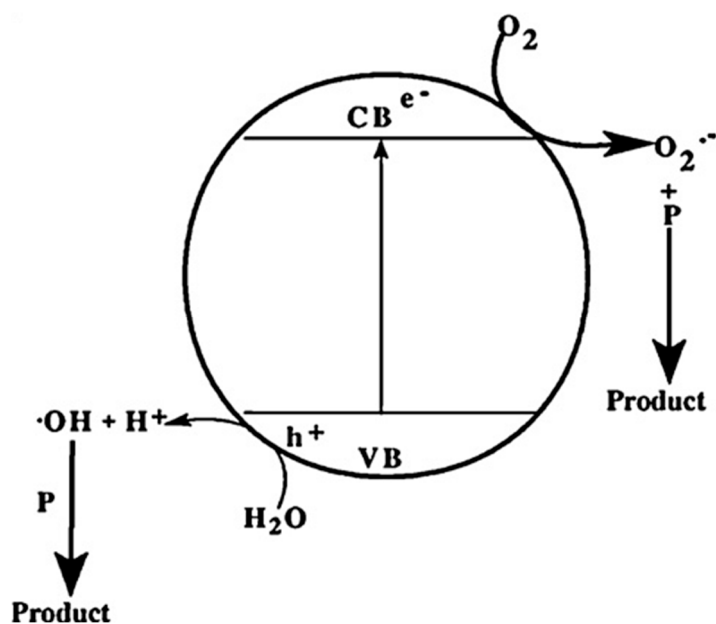
Figure 3. Simplified mechanism for the activation of a semiconductor by light. Adapted with permission from [61]. Copyright © 2010 Elsevier.
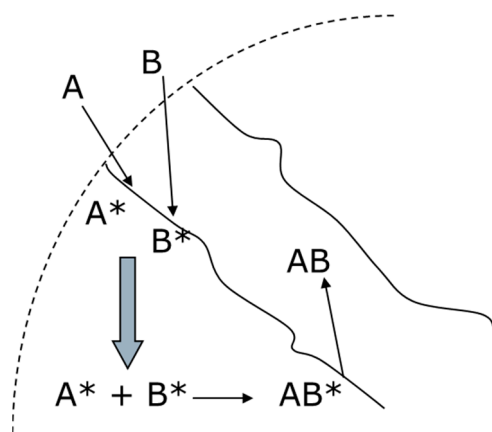

Figure 4. Schematic picture of the mechanism of heterogeneous photocatalysis.

2.2. Immobilized Photocatalysts for Azo Dye Degradation

A possible solution to avoiding the photocatalyst recovery step is immobilizing the semiconductors directly on the reactor walls in contact with the water to be treated and exposed to the light source [75,76]. However, it must be considered that the immobilization of photocatalysts on the reactor walls (as shown in Figure 5) or other parts of photocatalytic reactors has some drawbacks. Indeed, in the case of photoactivity decreases, it is challenging to remove and replace the photocatalysts [77]. Therefore, immobilizing the photocatalysts on macroscopic supports with a defined geometry (structured photocatalysts) that may be easily replaced in the photoreactors is the most cost-efficient method. Moreover, structured photocatalysts are permanently retained in the photocatalytic reactors [76], thus ensuring good contact between the liquid medium and the photocatalyst [77] and enhancing the photodegradation rate [78].
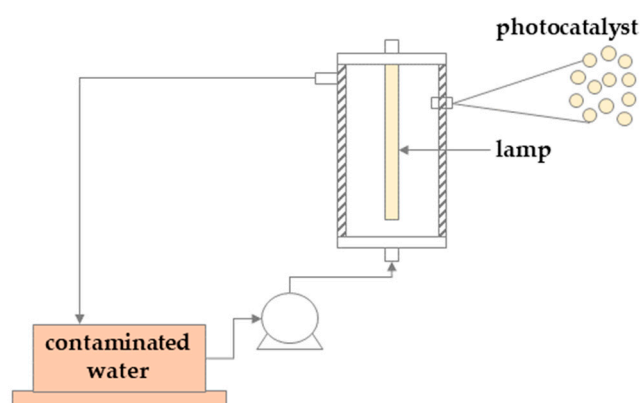
Figure 5. Simplified scheme of a photocatalytic system with a photocatalyst immobilized on the photoreactor wall.

From a practical point of view, the chosen support for photocatalysts must have the following features: strong adherence between the photocatalyst and support, no decrease in photocatalytic activity upon immobilization, a high specific surface area, and strong adsorption affinity towards the pollutants to be degraded [79–81].

The most studied support materials for immobilizing photocatalysts include glass, activated carbon, polymers, alumina, quartz, and some biodegradable materials (i.e., cellulose), among others [79]. Different techniques for preparing structured photocatalysts were also extensively reported in the literature. Some of these included the sol–gel process accomplished using dip coating steps [82,83], thermal treatment [84–86], chemical vapor deposition [87], electrodeposition [88,89], sol–spray deposition [90], and hydrothermal processes [91]. All such preparation methods were developed to anchor photocatalyst particles onto the chosen support stably, minimizing as much as possible the reduction in photocatalytic activity with respect to the photocatalyst in powder form [61]. Table 1 reports the catalytic performances of different photocatalysts immobilized on macroscopic supports and specifically formulated for the degradation of azo dyes in the last fifteen years.

Table 1. Catalytic performances of different photocatalysts immobilized on macroscopic supports. AO = Acid Orange; AR = Acid Red; COD = chemical oxygen demand; EB-T = Eriochrome Black T; MO = Methyl Orange; NR = Novacron Red; RO = Reactive Orange; TOC = total organic carbon; WW = wastewater.

Azo Dye	Photocatalyst	Light Source	Reactor	Degradation (%)	Treatment Time (min)	Ref.
MO	TiO_2/steel mesh	UVA	Batch	Total discoloration; TOC removal = 22% at pH = 6.8–7	180	[92]
AR 14	TiO_2/GO plate	UVA	Batch	Discoloration = 96.38% at pH = 9	120	[93]
RO 16	TiO_2:ZnO/3D fabric	UVC	Batch	Discoloration =96.38% in the presence of H_2O_2	60	[94]
AR 88	ZnO/glass plate	UVC	Batch	COD removal = 60%	240	[95]
MO	TiO_2/ceramic templates	UV	Batch	Discoloration of about 90%	210	[96]
MO	TiO_2/polyethersulfone film	UVA	Batch	Discoloration = 90%; TOC removal = 38% at pH = 5.8	540	[97]

Table 1. *Cont.*

Azo Dye	Photocatalyst	Light Source	Reactor	Degradation (%)	Treatment Time (min)	Ref.
EB-T	N-TiO$_2$/glass spheres	UVA Vis	Batch	Discoloration = 41% under UV light and 31% under visible light; TOC removal = 35% under UV light and 30% under visible light	210	[83]
MO	Ag@AgCl/ZnO on glass	Vis	Batch	Discoloration = 80.7%; TOC removal = 38% at pH = 5.8	120	[98]
MO	AgX/ZnO on glass	Vis	Batch	Discoloration = 84%	180	[91]
MO	Carbon/ ZnO on glass	UVC	Batch	Discoloration = 84%; TOC removal = 56% at pH = 5	95	[99]
EB-T	CdS/ZnO on glass	Vis	Batch	Discoloration = 45%	90	[100]
RO	ZnO/carbon fabric	UVA	Batch	Complete discoloration	100	[101]
MO	g-C$_3$N$_4$/ GO aerogel	Vis	Batch	Discoloration = 91.1%	40	[102]
MO	BaTiO$_3$ aerogels	UVA	Batch	Discoloration = 92.59% at pH = 3	120	[103]
MO	TiO$_2$/polypropylene fabrics	UV-Vis	Batch	Total discoloration	120	[104]
Tannery WW polluted by azo dyes	ZnO/glass spheres	UVA	Batch	COD removal = 70%	120	[86]
AO 7	N-TiO$_2$/polystyrene plate	Vis	Batch	Discoloration = 55%; TOC removal = 54%	180	[105]
AR 73	TiO$_2$/sackcloth fiber	UVA	Batch	Discoloration = 86%; COD removal = 96% at pH = 6.5	180	[57]
EB-T	TiO$_2$ pellets	UVA	Continuous	Complete discoloration	10 (steady-state condition)	[106]
NR	TiO$_2$/glass plate	UV	Continuous	Discoloration = 15% at pH = 7	350 (steady-state condition)	[107]

The data reported in Table 1 show that common macroscopic support materials for the immobilization of photocatalysts are glass spheres or glass plates [83,86,91,95,99,100,107], confirming that glass continues to be used as a support for most photocatalytic applications [79]. Indeed, it is well known that glass is permeable to UV and visible light, allowing high light transmission to the aqueous solutions. Therefore, no optical constraints influence the photoreactor design and operation [108]. Moreover, immobilizing photocatalysts on macroscopic glass supports is generally reflected in structured photocatalysts having good stability after several reuse cycles. For instance, in the paper by Vaiano et al., a N-doped TiO$_2$ (N-TiO$_2$) photocatalyst was immobilized on glass spheres through the sol–gel method and tested for its ability to degrade Eriocrome Black T under UV and visible-light irradiation, showing good photocatalytic activity both in the decolorization and in TOC removal [83]. Furthermore, the photocatalytic activity of TiO$_2$- and ZnO-based photocatalysts immobilized on a glass plate was also determined, and these photocatalysts were tested for their ability to remove different azo dyes [95,98,100,107], evaluating in some cases the stability of the catalytic systems after reuse cycles. In particular, Yu et al. [98] prepared Ag@AgCl/ZnO on a glass plate and tested the reusability of the optimized photocatalyst in the degradation of Methyl Orange (MO) and Methylene Blue (MB) (Figure 6).
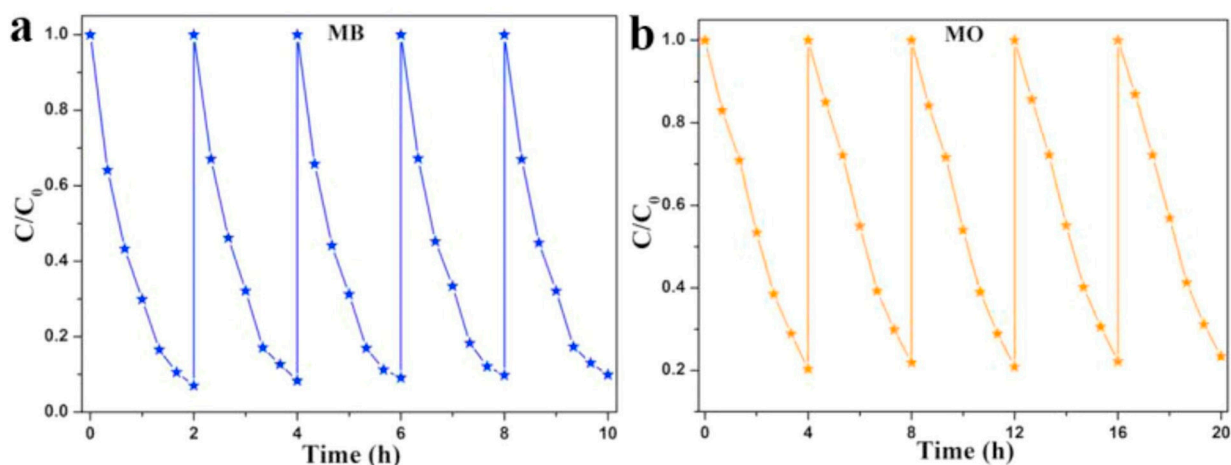
Figure 6. Four photodegradation reuse cycles of (**a**) MB and (**b**) MO with the optimized Ag@AgCl/ZnO on a glass plate. Adapted with permission from [98]. Copyright © 2018 Elsevier.

The photocatalytic discoloration performance of the optimized structured photocatalyst exhibited a negligible loss of photoactivity after four reuse cycles, highlighting its stability and reusability. Moreover, the authors reported scanning electron microscopy (SEM) images showing that the reused photocatalyst retained its original morphological structure.

In addition to glass media, carbon-based materials, such as graphene oxide (GO), were proposed as photocatalyst supports [102]. It is reported that these materials can ensure high dye degradation performances because of their chemical inertness, stability, large pore volume, large adsorption sites, and good thermal properties [79,109]. From this perspective, Tang et al. prepared a g-C$_3$N$_4$/GO aerogel hybrid with a macroscopic 3D architecture (Figure 7) for visible-light-driven degradation of MO [102].

Figure 7. Digital image of the g-C$_3$N$_4$/GO aerogel. Adapted with permission from [102]. Copyright © 2017 Elsevier.

The stability of the aerogel was tested through five photodegradation cycle runs (Figure 8).

It is possible to observe that MO photocatalytic degradation reached about 91% during the fifth run, within 40 min of the visible-light irradiation treatment. Based on such results, GO aerogel could be a suitable macroscopic support for visible-light-activated photocatalysts to quickly achieve a high photodegradation efficiency.

However, synthesizing graphene-based compounds is expensive, and their use could be recommended only for applications such as solar cells [108] and electronics devices [109] requiring high electrical conductivity.
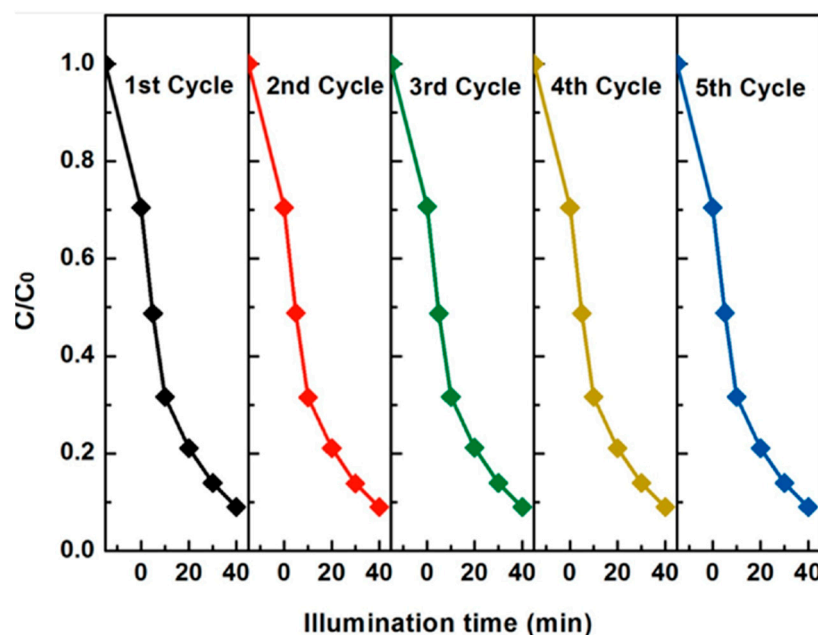
Figure 8. Photocatalytic stability of g-C$_3$N$_4$/GO aerogel in MO degradation over five cycle runs (a different color has been used to represent the lines related to different cycles). Reprinted with permission from [102]. Copyright © 2017 Elsevier.

It is possible to observe that MO photocatalytic degradation reached about 91% during the fifth run, within 40 min of the visible-light irradiation treatment. Based on such results, GO aerogel could be a suitable macroscopic support for visible-light-activated photocatalysts to quickly achieve a high photodegradation efficiency.

However, synthesizing graphene-based compounds is expensive, and their use could be recommended only for applications such as solar cells [108] and electronics devices [109] requiring high electrical conductivity.

For these reasons, polymeric materials (as well as aerogels) have gained much attention in recent years for their use in formulating structured photocatalysts [64,79,109]. Polymeric substances are relatively easy to prepare and inexpensive, chemically inert, mechanically stable, and durable [79,110–113]. Moreover, because of their low density, polymer supports can help formulate buoyant structured photocatalysts for water and wastewater treatment [111,114–117]. Compared with rigid substrates (such as glass, steel, and ceramic templates), polymeric materials are flexible and bendable, making them the second most common and practical support for the immobilization of different types of photocatalysts [109]. In this field, polyethersulfone-TiO$_2$ film photocatalysts were prepared using a phase inversion technique and used in the photocatalytic degradation of MO under UV light, achieving engaging removal performances (discoloration = 90%; TOC removal = 38% at pH = 5.8) [97].

Moreover, a buoyant photocatalyst consisting of TiO$_2$ immobilized on polypropylene fabrics was tested under UV-Vis light for the degradation of MO, achieving complete dye degradation after 120 min of treatment, whereas under only Vis light, MO degradation was about 90% after 240 min of irradiation [104]. Very recently, Sannino et al. [105] immobilized a visible-light-activated photocatalyst (N-TiO$_2$) in powder form on a transparent polystyrene plate (PS) using a simple solvent-assisted procedure. The obtained structured photocatalyst (N-TiO$_2$/PS) was placed in a photocatalytic reactor with a flat-plate geometry, irradiated by a matrix of 240 LEDs emitting Vis light to degrade Acid Orange 7 dye (AO7). The results show that, after 180 min of irradiation, the AO7 discoloration efficiency was unchanged (about 55%) after five reuse cycles (Figure 9), highlighting the stability of a structured photocatalyst realized with a polymer macroscopic support.
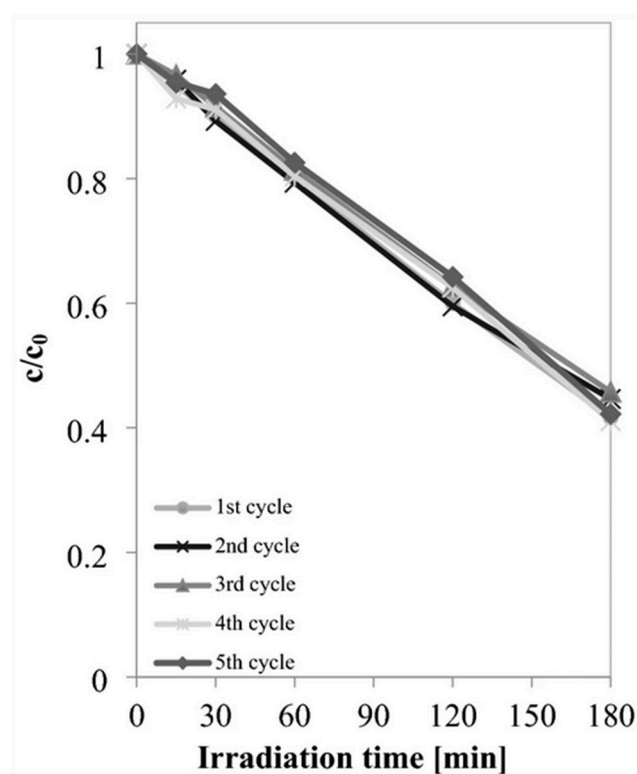
Figure 9. Stability of N-TiO$_2$/PS structured photocatalyst in AO7 discoloration. Adapted from [105].

Moreover, the final values of TOC removal efficiency (about 54%) were very close to the AO7 discoloration efficiency; thus, it could be argued that total conversion to CO$_2$ and water occurred thanks to a developed photocatalytic system (photoreactor with flat-plate geometry + N-TiO$_2$/PS structured photocatalyst).

In addition to polymeric films and plates, the use of polymer aerogels as supports for photocatalysts to be used in the degradation of water pollutants (including dyes) is also under investigation [64,118–122]. Polymer aerogels are extensively used in various applications, such as electrochemical and catalysis, because of their low toxicity, highly porous structure, buoyancy, and, therefore, ease of recovery [64,118,123,124]. In addition, photocatalyst particles can be entirely or partly embedded in the framework of polymer aerogels to minimize the leaching phenomena of photoactive phases from the support to the aqueous medium [118]. However, to date, most polymer aerogels have been used to remove various organic pollutants and rarely for azo dye photodegradation. For instance, Hasanpour et al. [125] studied the photocatalytic degradation of MO using a cellulose/ZnO aerogel (CA/ZnO) under UV light, showing complete dye discoloration after 120 min of irradiation. The optimized CA/ZnO system also effectively removed other types of dyes (Methylene Blue and Rhodamine B).

Another aspect to consider is the operational mode (batch or continuous) of the photoreactors in which the structured photocatalysts are placed. From Table 1, it can be seen that the most used photoreactors are in batch configuration. However, since batch treatment systems are not helpful for industrial applications of photocatalytic systems, there is growing interest in the design and development of continuous-flow photocatalytic reactors [106,126,127]. Indeed, photocatalytic reactors operating in the continuous mode are preferred because of the high demand for dye degradation in wastewater from textile industries, where a large volume of polluted water is generated by flow processes [107]. Among the continuous photoreactors, flow microreactors have received much attention, especially for photochemical reactions. Using photocatalytic microreactors allows for the uniform irradiation of the entire solution volume, and consequently, the photocatalytic degradation rate is markedly enhanced [128,129]. Microreactors can also improve the mass

transfer phenomena thanks to forming a thin film of polluted solution directly in contact with the surface of structured photocatalysts, thus ensuring an efficient penetration of light inside the core of the photoreactor [130]. Considering the specific case of azo dye photodegradation, Mohammed Redha et al. [107] studied the photocatalytic degradation of Novacron Red C-2BL in a miniaturized reactor (Figure 10) with an interchangeable TiO_2 nanofilm immobilized on a glass plate (40 × 25 × 1 mm) using the sol–gel dip coating method.
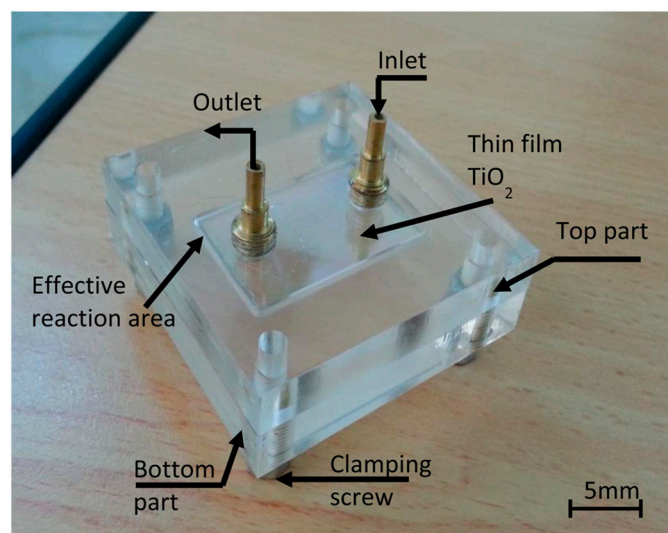

Figure 10. Miniaturized photocatalytic reactor for the degradation of Novacron Red C-2BL dye. Reprinted from [107].

The effect of different parameters, such as the pH, liquid flow rate, light intensity, amount of deposited TiO^2, and reaction temperature, was assessed. Under the optimized operating conditions, about 15% of the dye was degraded, but the steady-state conditions were reached after 350 min of run time. Much better photocatalytic degradation performances for two azo dyes were reported in the paper by Vaiano et al. [106]. Specifically, Eriochrome Black T (EBT) and MO were photodegraded in a continuous- flow photocatalytic microreactor irradiated by UV-LEDs and filled with TiO_2 pellets in a cylindrical shape (size: 12.5 mm × 5.5 mm) (Figure 11).
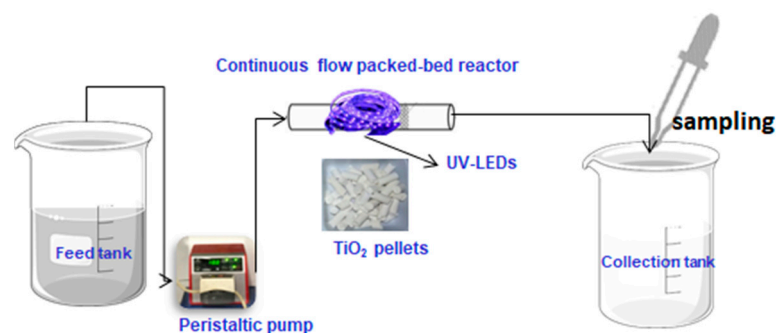

Figure 11. Schematic picture of the experimental apparatus based on continuous-flow photocatalytic microreactor irradiated by UV-LEDs and filled with TiO_2 pellets. Adapted with permission from [106]. Copyright © 2020 Elsevier.

The experimental results show that the best photocatalytic performances (EBT and MeO discoloration of about 100% and 90%, respectively) were achieved with a 0.5 mL/min liquid flow rate. It is essential to underline that with the continuous-flow photocatalytic packed-bed reactor proposed by Vaiano et al. [106], the steady-state conditions were reached after about 10 min of irradiation.

3. Supercritical Water Oxidation for Azo Dye Degradation

3.1. Fluids in Supercritical Conditions

Some innovative processes based on the use of supercritical fluids have found wide application in various research and industrial sectors [131,132]. A fluid is in the supercritical state when its pressure and temperature are higher than the critical values, as evident in the Pressure vs. Temperature diagram reported in Figure 12.
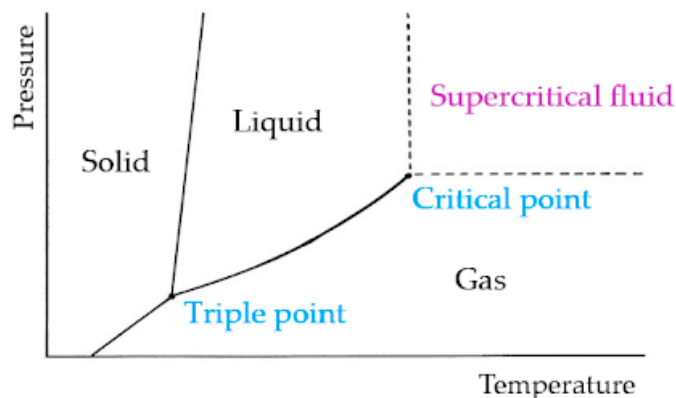

Figure 12. Pressure–temperature phase diagram.

Under these conditions, some properties of the substance are similar to those of a liquid (e.g., density or solvent power), and others are similar to those of a gas (e.g., viscosity or diffusivity) [133,134]. The substances mainly employed in the supercritical state are carbon dioxide [135,136] and water [137,138]. The processes based on the former (whose critical values are 31.1 °C for temperature and 7.38 MPa for pressure) are widely used in the processing of thermolabile compounds, such as pharmaceuticals [139] or foods [140]; the role of supercritical carbon dioxide is, in general, that of a co-solute, solvent, antisolvent, and foaming agent [141–144].

Supercritical water (SCW, critical temperature = 373.9 °C and critical pressure = 22.06 MPa) is mainly used as a reagent in processes such as SWG of biomass to produce hydrocarbon fuels [145], aqueous biomass stream conversion into clean water and gases [146], and SCW oxidation for the treatment of hazardous waste [147]. It is well known that water at standard pressure and temperature conditions is a suitable solvent for polar compounds. However, when it is in supercritical conditions, it behaves as an unassociated, non-polar solvent [148,149]; therefore, it becomes a good solvent for compounds that are not very soluble in water under ambient conditions, such as molecular oxygen, hydrogen, nitrogen, carbon monoxide, and numerous organic compounds [150].

3.2. Supercritical Water Oxidation

Supercritical water oxidation can convert organic substances into water and carbon dioxide in a single-phase reaction within short residence times (1–100 s) and with very high conversion rates (99–99.99%). The different polarity of water in supercritical conditions compared to water in ambient conditions plays a fundamental role in the presence of a single phase; indeed, many inorganic compounds, such as salts, are water-soluble at ambient conditions and only slightly soluble in SCW. This means that during the SCWO of industrial wastes, inorganics precipitate as solids for subsequent disposal [151]. The hetero-atoms of chlorine, sulfur, or phosphorus, which can be present in organic waste, are transformed into hydrochloric (HCl), sulfuric (H_2SO_4), and phosphoric (H_3PO_4) acids, respectively. Organic carbon is converted to carbon dioxide (not carbon monoxide), and organic and inorganic nitrogen mainly form N_2 and small amounts of N_2O. Unwanted by-products from incineration, such as dioxins or NO_x, are generally not formed [152].

SCWO has been studied since 1990 and developed at the industrial scale for treating industrial wastewater [153,154]. SCWO is an evolution of the well-established process of

wet air oxidation (WAO), in which the reaction process generally takes up to several hours; moreover, the complete removal of the organic material is very rarely achieved (in general, the efficiencies vary between 50% and 90%), with the need for subsequent treatments of the waste [155,156]. SCWO can be schematized considering four main steps: (1) pressurization of the reagents; (2) reaction; (3) salt separation; (4) depressurization and heat recovery. In the last step, it is necessary to use SCWO at an industrial scale because of the massive quantity of energy required to pressurize and preheat the reagents; indeed, the integration of the process allows energy to be recovered from the hot pressurized product stream for preheating or producing electricity [50]. A typical configuration of an SCWO plant is sketched in Figure 13 [157]. It is constituted of a feed tank, a high-pressure feed pump, a high-pressure air compressor, preheaters, a reactor, a cooling system, a back-pressure regulator, a gas–liquid separator, and sampling ports [158]. The plant schematized in Figure 13 is energetically self-sufficient because the reactor operates without any external energy supply. After all, the energy released in the reactor is used for the preheating step.
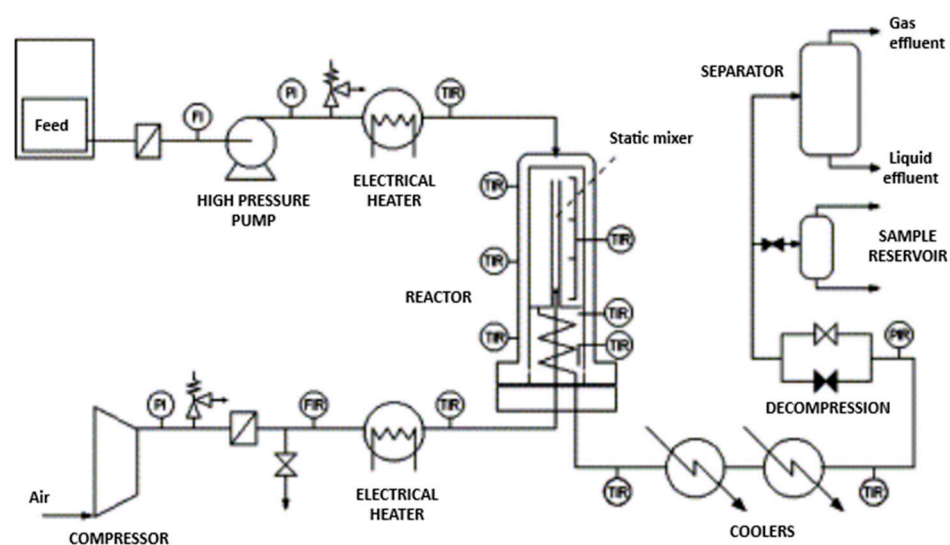

Figure 13. Sketch of an SCWO pilot plant. Adapted with permission from [157]. Copyright © 2002 Elsevier.

SCWO of Azo Dyes

Among its various applications, SCWO has been used to remove azo dyes from wastewater. Indeed, oxidative decolorization techniques often have a disadvantage in that the decomposition products are more toxic than the starting waste material; SCWO is characterized by minimized secondary toxicity [159] and is energy-efficient if the TOC content of the waste is higher than 10% [149].

A list of the main results obtained using SCWO in decolorizing textiles (in particular, those containing azo dyes) is reported in Table 2, in which, for each dye, the operating conditions and the main results obtained are indicated.

Table 2. SCWO main results with H_2O_2 as the oxygen source. BB = Basic Blue; COD = chemical oxygen demand; CV = Crystal Violet; DO = Disperse Orange; EBB = Eriochrome Blue Black; MB = Methylene Blue; MO = Methyl Orange; P = pressure; RB = Reactive Black; RBl = Reactive Blue; RO = Reactive Orange; RR = Reactive Red; t = residence time; T = temperature; TOC = total organic carbon; WW = wastewater.

Dye	P [MPa] T [°C] t [s]	Reactor	Main Results	Ref.
BB 41	P = 25 ± 1 T = 400–650 t = 9–19	Continuous	TOC removal efficiency up to 99.87%; complete degradation of BB41 and transformation into CO_2, H_2O, and their intermediate products	[160]
CV	P = 24 T = 275–500 t = 100–150	Batch	TOC degradation efficiency higher than 95% at temperatures higher than 385 °C with a removal efficiency up to 99.9% at 500 °C	[161]
DO 25	P = 25 ± 1 T = 400–600 t = 5–11	Continuous	COD conversion efficiency up to 98.5%; complete degradation of the molecular structure of DO25; clear and colorless water at temperatures higher than 500 °C	[162]
DO 25	P = 25 ± 1 T = 400–600 t = 5–11	Continuous	TOC removal efficiency up to 99.96%; liquid-phase products were clear and colorless at temperatures of 500 °C and above; they were clear and yellowish at 400 and 450 °C	[163]
EBB	P = 24 T = 275–500 t = 100–150	Batch	TOC degradation efficiency higher than 95% at temperatures higher than 300 °C with a removal efficiency up to 99.9% at 500 °C	[161]
MB	P = 24 T = 275–500 t = 100–150	Batch	TOC degradation efficiency higher than 95% at all the tested temperatures, with a removal efficiency up to 98% at 500 °C	[161]
MO	P = 24 T = 275–500 t = 100–150	Batch	TOC degradation efficiency higher than 95% at temperatures higher than 385 °C with a removal efficiency up to 99% at 500 °C	[161]
RB 5 RBl 49 RR 3	P = 30 T = 400 t = 600	Batch	Total decolorization of the dye was achieved at each dye concentration (TOC from 1 to 15%); an optimum 5–10% excess concentration is recommended for cost-effective SCWO of the reactive dyes studied; 99.9% TOC removal efficiency	[149]
RO 7	P = 25 ± 1 T = 400–550 t = 60–1200	Batch	COD conversion up to 98%; TOC removal efficiency up to 88%	[30]
RO 7	P = 25 T = 450–600 t = 600	Batch	COD and TOC decomposition efficiencies reached 99.6% and 93.9%, respectively	[164]
Textile WW	P = 25 T = 520–600 t = 120–600	Batch	COD removal efficiency up to 99.8%; catalytic SCWO strongly enhances the removal efficiency of COD and NH_3-N	[165]
Textile WW	P = 25 T = 400–600 t = 8–16	Continuous	TOC removal efficiency up to 100% and hydrothermal decomposition up to 93.8%; color of the WW removed completely at temperatures of 450 °C and above	[166]

Table 2. *Cont.*

Dye	P [MPa] T [°C] t [s]	Reactor	Main Results	Ref.
Textile WW	P = 22–30 T = 320–430 t = 13–34	Continuous	COD removal efficiency of more than 98.4% at the optimal reaction conditions	[29]
Textile WW	P = 25 T = 400–600 t = 15–45	Continuous	TOC conversions of the effluents after SCWO equal to 99.79% at the best reaction conditions	[167]

Observing the results reported in Table 2, it is evident that the pressure is, generally, in the range of 22–30 MPa, and the temperature is in the range of 400–600 °C; the reaction time depends on the type of reactor used: it is of the order of minutes in the case of batch reactors, and of the order of a few seconds in continuous reactors. The experiments are generally performed with an excess of oxygen (300–500%); this choice is commonly made because, due to the complexity of the wastewater dye, the amount of oxygen necessary to oxidize completely organic compounds in wastewater cannot be calculated using established chemical reaction equations. Indeed, some authors verified that the amount of intermediate products, such as methane, ethane, ethylene, propane, and propylene, decreased with excess oxygen [166]. The oxygen source is almost always hydrogen peroxide (H_2O_2) because of its aromatic ring-opening capability, which makes it more effective than other low-cost oxidants [168]. However, in some cases not reported in Table 2, oxygen [169] and air [157] have been used as oxidant agents.

In some studies, whose main results are reported in Table 2, one (or a few) azo compounds were removed from the water; in other cases, a mixture of compounds contained in the wastewater of the textile industry were considered. For example, Yang et al. [170] analyzed the SCWO of 14 N-containing compounds. Some azo dyes, such as Eriochrome Blue Black R (EBBR) and Methyl Orange (MO), have been studied. The reaction conditions were a residence time of 150 s, a stable pressure of 24 MPa, temperatures of 350–500 °C, and 500% excess oxygen, achieving a total nitrogen (TN) removal of up to 96%. Subsequently, the same group [171] investigated the SCWO of 41 organic compounds classified according to the different N-groups contained in the molecules. Among them, Crystal Violet (CV) and Basic Green (BG) were included in the -NH_2 group; EBBR, Orange G (OG), Acid Chrome Blue K (ACBK), and Solvent Red 23 (SR23) in the -N=N- group; and MO, Eriochrome Black T (EBT), Azure B, Acid Orange 74 (AO74), and alizarin yellow GG (AYGG) in the mixed group. SCWO was performed in a continuous reactor at 24 MPa and 450 °C with reaction times ranging from 30 s to 360 s and 500% excess oxygen; the TOC removal efficiencies were above 80% and even reached 100%, indicating that azo compounds were successfully decomposed through SCWO.

The evidence of color removal has often been documented in the literature by comparing the wastewater containing the dye and the treated water [160,164]. For example, Figure 14 shows the color change of water containing Basic Blue 41 dye (BB41) after SCWO at two different temperatures. In the experiment, which was performed at 450 °C, partial degradation of the dye was achieved (TOC decomposition equal to 77.76%), whereas when operating at 600 °C, the TOC decomposition rate was equal to 99.08% [160]. Correspondingly, the wastewater processed at 450 °C still showed residual color (Figure 14, vial in the middle), while the one from which the dye had been wholly removed appeared clear (Figure 14, vial on the right).

The complete removal of color is always achieved at relatively high temperatures. Söğüt and Akgün [166] observed that the color of a dyehouse wastewater containing several organic pollutants could be wholly removed at temperatures of at least 450 °C.

Figure 14. Basic Blue 41 solution (**left**) after oxidation at 450 °C (**middle**) and 600 °C (**right**). Reprinted with permission from [160]. Copyright © 2009 Elsevier.

An interesting finding was highlighted by Zhang et al. [30], who studied the reaction pathway of the azo group in the molecular structure of Reactive Orange 7 (RO 7) through theoretical analyses followed by experimental verification. These authors observed that nitrogen was mainly converted to gases and discharged, as opposed to ammonia, which was dissolved in liquid. This result seems to be in contrast with previously obtained results from the literature [172,173]; indeed, it has been frequently observed that nitrogen-containing compounds subjected to SCWO give as a final product nitrogen gas, which is refractory to SCWO, with ammonia as the primary reaction intermediate. In one study, in the case of aromatic azo compounds, which are characterized by high thermal stability, the azo group contained in RO7 was attacked by OH• and oxidized to the diazo group; the diazo compound, in the presence of water at high temperature and high pressure, promptly gave rise to a hydrolysis reaction:

$$Ar - N \equiv N + H_2O \rightarrow Ar - OH + N_2 + H$$
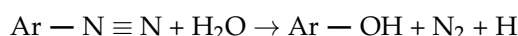
in which a hydroxyl group replaced the diazo groups with the formation of nitrogen and H^+ [30]. For this reason, ammonia nitrogen was scarcely produced during the SCWO of the azo dye under consideration.

Despite its very high performance in terms of conversion, SCWO has some drawbacks. Indeed, supercritical water causes corrosion, salt deposition, management of biphasic wastes, and plugging caused by the insolubility of mineral salts above the critical point; this aspect reduces the efficiency of the chemical reaction and sometimes blocks the process.

Several attempts have been made to overcome these limits by following different approaches. For example, Zhang et al. [30] used a lining made of stainless steel 316 to cover the inner surface of the reactor to avoid body corrosion. Bermejo et al. [174] designed different transpiring wall reactors in which the reaction chamber was limited by a porous sintered AISI 316 wall. Clean and cold water, flowing continuously through the wall, creates a thin layer that protects the wall against corrosion and salt deposition. They compared the performance of different configurations, such as a fully porous wall and two partially porous walls made of a porous sintered alloy and a nonporous alloy. The best results in terms of temperature resistance and protection of the wall were obtained with the latter design.

For these reasons, in recent years, catalytic subcritical water oxidation (CSCWO) has been catching on [6]. Indeed, using a catalyst can decrease the experimental temperature and pressure conditions and the reaction time, thereby decreasing the size of the reactor

and heat exchanger, and ultimately reducing the total cost of the process. However, CSCWO involves using a catalyst to accelerate the oxidation of organic compounds with the consequent introduction of additional costs and the need for regeneration and replacement of the catalyst itself. From the point of view of applicability, SCWO is most effective method for waste streams with a high organic content, while CSCWO is more suitable for waste streams with a lower organic content.

SCWO is underdeveloped on an industrial scale because of some technical aspects [51] related to:

- The high amount of energy required for the start-up of the process, which can be overcome by running the process for extended periods;
- The stringent thermal control necessary to retain safe conditions and carry out optimal energy recovery, which can be achieved using cooling water injections in various positions along the reactor;
- The possible erosion of the internal parts of the back-pressure regulator valves due to suspended solid particles contained in the wastewater that can create problems during the depressurization step.

4. Conclusions and Perspectives

Regarding heterogeneous photocatalysis, this review paper summarizes the advancements in photocatalysts immobilized on macroscopic supports (structured photocatalysts) for the degradation of azo dyes. Various important features of structured photocatalysts and their photocatalytic efficiency have been discussed.

Based on the literature analysis, some aspects of possible future research are reported in the following:

1. Due to their high light transmission and chemical stability, glass materials (such as glass spheres and glass plates) are still the most commonly reported supports for photocatalysts. Still, they have been used for the degradation of azo dyes mainly at the laboratory scale, and their effectiveness at the industrial scale still has to be proven.

2. Besides glass substrates, polymeric materials (in the form of films or plates) are effective supports for structured photocatalysts utilized for azo dye degradation. However, in recent years, monolithic polymer aerogels with photocatalytic properties have been shown to be promising materials for wastewater treatment since these materials present exciting features, such as a high porosity, high specific surface area, low density, and easy separation from the treated water. Despite such advantages, to date, most polymer aerogels have been used to remove a wide variety of organic pollutants and rarely for azo dye photodegradation. Therefore, specific research studies on using these materials for colored wastewater are recommended.

3. Studies on structured photocatalysts have been carried out to enhance their photocatalytic performances in dye degradation, achieving, in most cases, high removal only after prolonged irradiation time. Therefore, it is necessary to investigate the possibility of coupling photocatalytic processes based on structured photocatalysts with other treatment technologies (e.g., adsorption) to maximize the removal efficiency at a very low treatment time.

4. Previous works are mainly based on the use of batch photocatalytic reactors. However, since batch treatment systems are not recommended for industrial applications of photocatalytic systems in actual practice, developing continuous-flow photocatalytic reactors with a high efficiency in degrading azo dyes is desirable. From this perspective, it was reported that using microreactors allows the entire solution volume to be irradiated uniformly, substantially enhancing the photodegradation performances. However, photocatalytic microreactors only work with meager liquid flow rates, typically 3–6 mL/min. These values are far from the typical values for wastewater coming from textile industries. Therefore, future research papers should focus on the

design, scaling up, and feasibility demonstrations of photocatalytic microreactors for industrial applications, specifically for treating wastewater polluted by azo dyes.

Supercritical water oxidation has been used to remove azo dyes from wastewater using batch and continuous reactors. Different authors have observed that, with respect to water at ambient conditions, supercritical water allows the dissolution of many organic compounds because of their differing polarities in supercritical conditions. SCWO can convert the organic substances in wastewater into water and carbon dioxide in a single-phase reaction and with an almost complete (99–99.99%) conversion rate. The operating conditions tested by the various authors processing different azo dyes are not very different from each other: indeed, the pressure is, generally, in the range of 22–30 MPa, and the temperature in the range of 400–600 °C. The reaction time depends on the reactor type: it is of the order of minutes (1–20 min) in the case of batch reactors and of the order of a few seconds (5–45 s) in continuous reactors. The experiments are generally performed with an excess of oxygen (300–500%) to ensure the conversion is as complete as possible. In this review paper, the limits of SCWO and the possible strategies contrived by researchers to overcome them (such as using reactors with transpiring walls to avoid corrosion of equipment and pipes) have also been highlighted.

References

1. Christie, R.M. *Colour Chemistry*; Royal Society of Chemistry: London, UK, 2014; ISBN 1849733287.
2. Benkhaya, b.; El Harfi, S.; El Harfi, A. Classifications, properties and applications of textile dyes: A review. *Appl. J. Environ. Eng. Sci.* **2017**, *3*, 311–320. [CrossRef]
3. Benkhaya, S.; M'Rabet, S.; El Harfi, A. Classifications, properties, recent synthesis and applications of azo dyes. *Heliyon* **2020**, *6*, e03271. [CrossRef] [PubMed]
4. Gürses, A.; Açıkyıldız, M.; Güneş, K.; Gürses, M.S.; Gürses, A.; Açıkyıldız, M.; Güneş, K.; Gürses, M.S. Classification of dye and pigments. In *Dyes and Pigments*; Springer: Cham, Switzerland, 2016. [CrossRef]
5. Rauf, M.A.; Meetani, M.A.; Hisaindee, S. An overview on the photocatalytic degradation of azo dyes in the presence of TiO_2 doped with selective transition metals. *Desalination* **2011**, *276*, 13–27. [CrossRef]
6. Javaid, R.; Qazi, U.Y.; Ikhlaq, A.; Zahid, M.; Alazmi, A. Subcritical and supercritical water oxidation for dye decomposition. *J. Environ. Manag.* **2021**, *290*, 112605. [CrossRef] [PubMed]
7. Oyetade, J.A.; Machunda, R.L.; Hilonga, A. Photocatalytic degradation of azo dyes in textile wastewater by Polyaniline composite catalyst-a review. *Sci. Afr.* **2022**, *17*, e01305. [CrossRef]
8. Bafana, A.; Devi, S.S.; Chakrabarti, T. Azo dyes: Past, present and the future. *Environ. Rev.* **2011**, *19*, 350–370. [CrossRef]
9. Benkhaya, S.; M'rabet, S.; El Harfi, A. A review on classifications, recent synthesis and applications of textile dyes. *Inorg. Chem. Commun.* **2020**, *115*, 107891. [CrossRef]
10. Akinropo, O.J.; Oluwafemi, A.; Olumide, A. Tensile Properties and Dye Uptake Assessment of Cotton Fabrics Sized with Corn (*Zea mays*) Starch and Sorghum (*Sorghum bicolor*) Starch. *Earthline J. Chem. Sci.* **2021**, *5*, 49–62. [CrossRef]
11. Saini, R.D. Textile organic dyes: Polluting effects and elimination methods from textile waste water. *Int. J. Chem. Eng. Res.* **2017**, *9*, 121–136.
12. Konstantinou, I.K.; Albanis, T.A. TiO_2-assisted photocatalytic degradation of azo dyes in aqueous solution: Kinetic and mechanistic investigations: A review. *Appl. Cat. B* **2004**, *49*, 1–14. [CrossRef]
13. Muhd Julkapli, N.; Bagheri, S.; Bee Abd Hamid, S. Recent advances in heterogeneous photocatalytic decolorization of synthetic dyes. *Sci. World J.* **2014**, *2014*, 692307. [CrossRef] [PubMed]
14. Jie, R.H.; Guo, G.B.; Zhao, W.G.; An, S.L. Preparation and photocatalytic degradation for methyl orange of nano-powder TiO_2 by hydrothermal method supported on activated carbon. *Rengong Jingti Xuebao* **2013**, *42*, 2144–2149.

15. Bouberka, Z.; Benabbou, K.A.; Khenifi, A.; Maschke, U. Degradation by irradiation of an Acid Orange 7 on colloidal TiO 2/(LDHs). *J. Photochem. Photobiol. A* **2014**, *275*, 21–29. [CrossRef]

16. He, L.; Freeman, H.S.; Lu, L.; Zhang, S. Spectroscopic study of anthraquinone dye/amphiphile systems in binary aqueous/organic solvent mixtures. *Dye. Pigment.* **2011**, *91*, 389–395. [CrossRef]

17. Sharma, A.; Rani, S.; Bansal, A.; Sood, A. Effect of mordant combination on silk dyeing with apricot dye. In *Natural Dyes: Scope Challenges*; Daniel, M., Bhattacharya, S.D., Arya, A., Raole, V.M., Eds.; Scientific Publishers (India): Jodhpur, India, 2006; pp. 137–143.

18. Harbinder, K.; Namrita, K. Eco-friendly finishing and dyeing of jute with direct and mordant dye method. *Asian J. Home Sci.* **2012**, *7*, 19–22.

19. Lau, Y.Y.; Wong, Y.S.; Teng, T.T.; Morad, N.; Rafatullah, M.; Ong, S.A. Coagulation-flocculation of azo dye acid orange 7 with green refined laterite soil. *Chem. Eng. J.* **2014**, *246*, 383–390. [CrossRef]

20. Obiora-Okafo, I.; Onukwuli, O. Optimization of coagulation-flocculation process for colour removal from azo dye using natural polymers: Response surface methodological approach. *Niger. J. Technol.* **2017**, *36*, 482–495. [CrossRef]

21. Nazir, R.; Khan, M.; Rehman, R.U.; Shujah, S.; Khan, M.; Ullah, M.; Zada, A.; Mahmood, N.; Ahmad, I. Adsorption of selected azo dyes from an aqueous solution by activated carbon derived from *Monotheca buxifolia* waste seeds. *Soil Water Res.* **2020**, *15*, 166–172. [CrossRef]

22. Chen, M.; Ding, W.; Wang, J.; Diao, G. Removal of azo dyes from water by combined techniques of adsorption, desorption, and electrolysis based on a supramolecular sorbent. *Ind. Eng. Chem. Res.* **2013**, *52*, 2403–2411. [CrossRef]

23. Mittal, Y.; Dash, S.; Srivastava, P.; Mishra, P.M.; Aminabhavi, T.M.; Yadav, A.K. Azo dye containing wastewater treatment in earthen membrane based unplanted two chambered constructed wetlands-microbial fuel cells: A new design for enhanced performance. *Chem. Eng. J.* **2022**, *427*, 131856. [CrossRef]

24. Pan, Y.; Wang, Y.; Zhou, A.; Wang, A.; Wu, Z.; Lv, L.; Li, X.; Zhang, K.; Zhu, T. Removal of azo dye in an up-flow membrane-less bioelectrochemical system integrated with bio-contact oxidation reactor. *Chem. Eng. J.* **2017**, *326*, 454–461. [CrossRef]

25. Pandey, A.; Singh, P.; Iyengar, L. Bacterial decolorization and degradation of azo dyes. *Int. Biodeterior. Biodegrad.* **2007**, *59*, 73–84. [CrossRef]

26. Solís, M.; Solís, A.; Pérez, H.I.; Manjarrez, N.; Flores, M. Microbial decolouration of azo dyes: A review. *Process Biochem.* **2012**, *47*, 1723–1748. [CrossRef]

27. Hinckley, D.A.; Seybold, P.G.; Borris, D.P. Solvatochromism and thermochromism of rhodamine solutions. *Spectrochim. Acta Part A Mol. Spectrosc.* **1986**, *42*, 747–754. [CrossRef]

28. Devi, L.G.; Arunakumari, M.L. Enhanced photocatalytic performance of Hemin (chloro(protoporhyinato) iron(III)) anchored TiO$_2$ photocatalyst for methyl orange degradation: A surface modification method. *Appl. Surf. Sci.* **2013**, *276*, 521–528. [CrossRef]

29. Gong, W.-J.; Li, F.; Xi, D.-L. Oxidation of Industrial Dyeing Wastewater by Supercritical Water Oxidation in Transpiring-Wall Reactor. *Water Environ. Res.* **2008**, *80*, 186–192. [CrossRef]

30. Zhang, J.; Wang, S.; Guo, Y.; Xu, D.; Gong, Y.; Tang, X. Experimental study on supercritical water oxidation of CI Reactive Orange7 dye wastewater using response surface methodology. *Colour. Technol.* **2012**, *128*, 323–330. [CrossRef]

31. Al-Tohamy, R.; Ali, S.S.; Li, F.; Okasha, K.M.; Mahmoud, Y.A.G.; Elsamahy, T.; Jiao, H.; Fu, Y.; Sun, J. A critical review on the treatment of dye-containing wastewater: Ecotoxicological and health concerns of textile dyes and possible remediation approaches for environmental safety. *Ecotoxicol. Environ. Saf.* **2022**, *231*, 113160. [CrossRef]

32. Kishor, R.; Purchase, D.; Saratale, G.D.; Saratale, R.G.; Ferreira, L.F.R.; Bilal, M.; Chandra, R.; Bharagava, R.N. Ecotoxicological and health concerns of persistent coloring pollutants of textile industry wastewater and treatment approaches for environmental safety. *J. Environ. Chem. Eng.* **2021**, *9*, 105012. [CrossRef]

33. Huo, Y.; Xie, Z.; Wang, X.; Li, H.; Hoang, M.; Caruso, R.A. Methyl orange removal by combined visible-light photocatalysis and membrane distillation. *Dye. Pigment.* **2013**, *98*, 106–112. [CrossRef]

34. Vogelpohl, A.; Kim, S.-M. Advanced oxidation processes (AOPs) in wastewater treatment. *J. Ind. Eng. Chem.* **2004**, *10*, 33–40.

35. Silva, A.C.; Pic, J.S.; Sant'Anna, G.L., Jr.; Dezotti, M. Ozonation of azo dyes (Orange II and Acid Red 27) in saline media. *J. Hazard. Mater.* **2009**, *169*, 965–971. [CrossRef] [PubMed]

36. Ay, F.; Catalkaya, E.C.; Kargi, F. A statistical experiment design approach for advanced oxidation of Direct Red azo-dye by photo-Fenton treatment. *J. Hazard. Mater.* **2009**, *162*, 230–236. [CrossRef]

37. Tarkwa, J.B.; Oturan, N.; Acayanka, E.; Laminsi, S.; Oturan, M.A. Photo-Fenton oxidation of Orange G azo dye: Process optimization and mineralization mechanism. *Environ. Chem. Lett.* **2019**, *17*, 473–479. [CrossRef]

38. Iervolino, G.; Vaiano, V.; Sannino, D.; Rizzo, L.; Galluzzi, A.; Polichetti, M.; Pepe, G.; Campiglia, P. Hydrogen production from glucose degradation in water and wastewater treated by Ru-LaFeO3/Fe2O3 magnetic particles photocatalysis and heterogeneous photo-Fenton. *Int. J. Hydrogen Energy* **2018**, *43*, 2184–2196. [CrossRef]

39. Bahadori, E.; Vaiano, V.; Esposito, S.; Armandi, M.; Sannino, D.; Bonelli, B. Photo-activated degradation of tartrazine by H2O2 as catalyzed by both bare and Fe-doped methyl-imogolite nanotubes. *Catal. Today* **2018**, *304*, 199–207. [CrossRef]

40. Ince, N.H.; Gönenç, D.T. Treatability of a textile azo dye by uv/h2o2. *Environ. Technol.* **1997**, *18*, 179–185. [CrossRef]

41. Muruganandham, M.; Swaminathan, M. Photochemical oxidation of reactive azo dye with UV-H2O2 process. *Dye. Pigment.* **2004**, *62*, 269–275. [CrossRef]

42. Iervolino, G.; Vaiano, V.; Pepe, G.; Campiglia, P.; Palma, V. Degradation of acid orange 7 azo dye in aqueous solution by a catalytic-assisted, non-thermal plasma process. *Catalysts* **2020**, *10*, 888. [CrossRef]

43. Russo, M.; Iervolino, G.; Vaiano, V.; Palma, V. Non-thermal plasma coupled with catalyst for the degradation of water pollutants: A review. *Catalysts* **2020**, *10*, 1438. [CrossRef]

44. Garcia-Segura, S.; Dosta, S.; Guilemany, J.M.; Brillas, E. Solar photoelectrocatalytic degradation of Acid Orange 7 azo dye using a highly stable TiO_2 photoanode synthesized by atmospheric plasma spray. *Appl. Cat. B* **2013**, *132–133*, 142–150. [CrossRef]

45. Ferraz, E.R.A.; Oliveira, G.A.R.; Grando, M.D.; Lizier, T.M.; Zanoni, M.V.B.; Oliveira, D.P. Photoelectrocatalysis based on Ti/TiO_2 nanotubes removes toxic properties of the azo dyes Disperse Red 1, Disperse Red 13 and Disperse Orange 1 from aqueous chloride samples. *J. Environ. Manag.* **2013**, *124*, 108–114. [CrossRef] [PubMed]

46. Al-Rasheed, R.A. Water treatment by heterogeneous photocatalysis an overview. In Proceedings of the 4th SWCC Acquired experience symposium, Jeddah, Saudi Arabia, 7 May 2005; pp. 1–14.

47. Neppolian, B.; Choi, H.C.; Sakthivel, S.; Arabindoo, B.; Murugesan, V. Solar light induced and TiO_2 assisted degradation of textile dye reactive blue 4. *Chemosphere* **2002**, *46*, 1173–1181. [CrossRef] [PubMed]

48. Stylidi, M.; Kondarides, D.I.; Verykios, X.E. Pathways of solar light-induced photocatalytic degradation of azo dyes in aqueous TiO_2 suspensions. *Appl. Cat. B* **2003**, *40*, 271–286. [CrossRef]

49. Jiang, Z.; Li, Y.; Wang, S.; Cui, C.; Yang, C.; Li, J. Review on mechanisms and kinetics for supercritical water oxidation processes. *Appl. Sci.* **2020**, *10*, 4937. [CrossRef]

50. Bermejo, M.D.; Cocero, M.J. Supercritical water oxidation: A technical review. *AIChE J.* **2006**, *52*, 3933–3951. [CrossRef]

51. Vadillo, V.; Sánchez-Oneto, J.; Portela, J.R.; Martínez De La Ossa, E.J. Problems in supercritical water oxidation process and proposed solutions. *Ind. Eng. Chem. Res.* **2013**, *52*, 7617–7629. [CrossRef]

52. Veriansyah, B.; Kim, J.D. Supercritical water oxidation for the destruction of toxic organic wastewaters: A review. *J. Environ. Sci. (China)* **2007**, *19*, 513–522. [CrossRef]

53. Shanableh, A. Production of useful organic matter from sludge using hydrothermal treatment. *Water Res.* **2000**, *34*, 945–951. [CrossRef]

54. Nishio, J.; Tokumura, M.; Znad, H.T.; Kawase, Y. Photocatalytic decolorization of azo-dye with zinc oxide powder in an external UV light irradiation slurry photoreactor. *J. Hazard. Mater.* **2006**, *138*, 106–115. [CrossRef]

55. Weldegebrieal, G.K. Synthesis method, antibacterial and photocatalytic activity of ZnO nanoparticles for azo dyes in wastewater treatment: A review. *Inorg. Chem. Commun.* **2020**, *120*, 108140. [CrossRef]

56. Iervolino, G.; Zammit, I.; Vaiano, V.; Rizzo, L. Limitations and Prospects for Wastewater Treatment by UV and Visible-Light-Active Heterogeneous Photocatalysis: A Critical Review. *Top. Curr. Chem.* **2019**, *378*, 7. [CrossRef] [PubMed]

57. Vaez, M.; Zarringhalam Moghaddam, A.; Alijani, S. Optimization and modeling of photocatalytic degradation of azo dye using a response surface methodology (RSM) based on the central composite design with immobilized Titania nanoparticles. *Ind. Eng. Chem. Res.* **2012**, *51*, 4199–4207. [CrossRef]

58. Coronado, J.M.; Fresno, F.; Hernández-Alonso, M.D.; Portela, R. Design of advanced photocatalytic materials for energy and environmental applications. In *Green Energy and Technology*; Springer: Berlin/Heidelberg, Germany, 2013; Volume 71.

59. Franco, P.; Sacco, O.; De Marco, I.; Sannino, D.; Vaiano, V. Photocatalytic Degradation of Eriochrome Black-T Azo Dye Using Eu-Doped ZnO Prepared by Supercritical Antisolvent Precipitation Route: A Preliminary Investigation. *Top. Catal.* **2020**, *63*, 1193–1205. [CrossRef]

60. Mottola, S.; Mancuso, A.; Sacco, O.; De Marco, I.; Vaiano, V. Production of hybrid TiO_2/β-CD photocatalysts by supercritical antisolvent micronization for UV light-driven degradation of azo dyes. *J. Supercrit. Fluids* **2022**, *188*, 105695. [CrossRef]

61. Shan, A.Y.; Ghazi, T.I.M.; Rashid, S.A. Immobilisation of titanium dioxide onto supporting materials in heterogeneous photocatalysis: A review. *Appl. Cat. A* **2010**, *389*, 1–8. [CrossRef]

62. Hoffmann, M.R.; Martin, S.T.; Choi, W.; Bahnemann, D.W. Environmental Applications of Semiconductor Photocatalysis. *Chem. Rev.* **1995**, *95*, 69–96. [CrossRef]

63. Ibhadon, A.O.; Fitzpatrick, P. Heterogeneous Photocatalysis: Recent Advances and Applications. *Catalysts* **2013**, *3*, 189–218. [CrossRef]

64. Hasanpour, M.; Hatami, M. Photocatalytic performance of aerogels for organic dyes removal from wastewaters: Review study. *J. Mol. Liq.* **2020**, *309*, 113094. [CrossRef]

65. Ansari, S.A.; Ansari, S.G.; Foaud, H.; Cho, M.H. Facile and sustainable synthesis of carbon-doped ZnO nanostructures towards the superior visible light photocatalytic performance. *New J. Chem.* **2017**, *41*, 9314–9320. [CrossRef]

66. Yao, S.; Qu, F.; Wang, G.; Wu, X. Facile hydrothermal synthesis of WO3 nanorods for photocatalysts and supercapacitors. *J. Alloys Compd.* **2017**, *724*, 695–702. [CrossRef]

67. Pitre, S.P.; Yoon, T.P.; Scaiano, J.C. Titanium dioxide visible light photocatalysis: Surface association enables photocatalysis with visible light irradiation. *Chem. Commun.* **2017**, *53*, 4335–4338. [CrossRef] [PubMed]

68. Sun, W.; Meng, Q.; Jing, L.; Liu, D.; Cao, Y. Facile synthesis of surface-modified nanosized α-Fe2O 3 as efficient visible photocatalysts and mechanism insight. *J. Phys. Chem. C* **2013**, *117*, 1358–1365. [CrossRef]

69. Bae, J.; Kim, J.; Jeong, H.; Lee, H. CO oxidation on SnO_2 surfaces enhanced by metal doping. *Catal. Sci. Technol.* **2018**, *8*, 782–789. [CrossRef]

70. Arabzadeh, A.; Salimi, A. One dimensional CdS nanowire@TiO₂ nanoparticles core-shell as high performance photocatalyst for fast degradation of dye pollutants under visible and sunlight irradiation. *J. Colloid Interface Sci.* **2016**, *479*, 43–54. [CrossRef]

71. Sacco, O.; Franco, P.; De Marco, I.; Vaiano, V.; Callone, E.; Ceccato, R.; Parrino, F. Photocatalytic activity of Eu-doped ZnO prepared by supercritical antisolvent precipitation route: When defects become virtues. *J. Mater. Sci. Technol.* **2022**, *112*, 49–58. [CrossRef]

72. Vaiano, V.; Sacco, O.; Matarangolo, M. Photocatalytic degradation of paracetamol under UV irradiation using TiO₂-graphite composites. *Catal. Today* **2018**, *315*, 230–236. [CrossRef]

73. Khataee, A.R.; Pons, M.N.; Zahraa, O. Photocatalytic degradation of three azo dyes using immobilized TiO₂ nanoparticles on glass plates activated by UV light irradiation: Influence of dye molecular structure. *J. Hazard. Mater.* **2009**, *168*, 451–457. [CrossRef]

74. Behnajady, M.A.; Modirshahla, N.; Daneshvar, N.; Rabbani, M. Photocatalytic degradation of an azo dye in a tubular continuous-flow photoreactor with immobilized TiO₂ on glass plates. *Chem. Eng. J.* **2007**, *127*, 167–176. [CrossRef]

75. Krýsa, J.; Novotná, P.; Kment, S.; Mills, A. Effect of glass substrate and deposition technique on the properties of sol gel TiO₂ thin films. *J. Photochem. Photobiol. A* **2011**, *222*, 81–86. [CrossRef]

76. Joseph, A.; Vijayanandan, A. Review on support materials used for immobilization of nano-photocatalysts for water treatment applications. *Inorg. Chim. Acta* **2023**, *545*, 121284. [CrossRef]

77. Wang, J.; Zhao, J.; Sun, L.; Wang, X. A review on the application of photocatalytic materials on textiles. *Text. Res. J.* **2015**, *85*, 1104–1118. [CrossRef]

78. Zulfakar, M.; Hairul, N.A.H.; Akmal, H.M.R.; Rahman, M.A. Photocatalytic degradation of phenol in a fluidized bed reactor utilizing immobilized TiO₂ photocatalyst: Characterization and process studies. *J. Appl. Sci.* **2011**, *11*, 2320–2326. [CrossRef]

79. Srikanth, B.; Goutham, R.; Badri Narayan, R.; Ramprasath, A.; Gopinath, K.P.; Sankaranarayanan, A.R. Recent advancements in supporting materials for immobilised photocatalytic applications in waste water treatment. *J. Environ. Manag.* **2017**, *200*, 60–78. [CrossRef] [PubMed]

80. Li Puma, G.; Bono, A.; Krishnaiah, D.; Collin, J.G. Preparation of titanium dioxide photocatalyst loaded onto activated carbon support using chemical vapor deposition: A review paper. *J. Hazard. Mater.* **2008**, *157*, 209–219. [CrossRef] [PubMed]

81. Pozzo, R.L.; Baltanás, M.A.; Cassano, A.E. Supported titanium oxide as photocatalyst in water decontamination: State of the art. *Catal. Today* **1997**, *39*, 219–231. [CrossRef]

82. Sonawane, R.S.; Hegde, S.G.; Dongare, M.K. Preparation of titanium(IV) oxide thin film photocatalyst by sol–gel dip coating. *Mater. Chem. Phys.* **2003**, *77*, 744–750. [CrossRef]

83. Vaiano, V.; Sacco, O.; Sannino, D.; Ciambelli, P. Nanostructured N-doped TiO₂ coated on glass spheres for the photocatalytic removal of organic dyes under UV or visible light irradiation. *Appl. Cat. B* **2015**, *170–171*, 153–161. [CrossRef]

84. Cao, S.; Liu, B.; Fan, L.; Yue, Z.; Liu, B.; Cao, B. Highly antibacterial activity of N-doped TiO₂ thin films coated on stainless steel brackets under visible light irradiation. *Appl. Surf. Sci.* **2014**, *309*, 119–127. [CrossRef]

85. Ebrahimi, R.; Maleki, A.; Zandsalimi, Y.; Ghanbari, R.; Shahmoradi, B.; Rezaee, R.; Safari, M.; Joo, S.W.; Daraei, H.; Harikaranahalli Puttaiah, S.; et al. Photocatalytic degradation of organic dyes using WO3-doped ZnO nanoparticles fixed on a glass surface in aqueous solution. *J. Ind. Eng. Chem.* **2019**, *73*, 297–305. [CrossRef]

86. Vaiano, V.; Iervolino, G. Facile method to immobilize ZnO particles on glass spheres for the photocatalytic treatment of tannery wastewater. *J. Colloid Interface Sci.* **2018**, *518*, 192–199. [CrossRef] [PubMed]

87. Carp, O.; Huisman, C.L.; Reller, A. Photoinduced reactivity of titanium dioxide. *Prog. Solid State Chem.* **2004**, *32*, 33–177. [CrossRef]

88. Xu, F.; Shen, Y.; Sun, L.; Zeng, H.; Lu, Y. Enhanced photocatalytic activity of hierarchical ZnO nanoplate-nanowire architecture as environmentally safe and facilely recyclable photocatalyst. *Nanoscale* **2011**, *3*, 5020–5025. [CrossRef]

89. Djošić, M.S.; Mišković-Stanković, V.B.; Janaćković, D.T.; Kačarević-Popović, Z.M.; Petrović, R.D. Electrophoretic deposition and characterization of boehmite coatings on titanium substrate. *Colloids Surf. A Physicochem. Eng. Asp.* **2006**, *274*, 185–191. [CrossRef]

90. Chen, C.H.; Kelder, E.M.; Schoonman, J. Electrostatic sol-spray deposition (ESSD) and characterisation of nanostructured TiO₂ thin films. *Thin Solid Films* **1999**, *342*, 35–41. [CrossRef]

91. Lu, J.; Wang, H.; Dong, Y.; Wang, F.; Dong, S. Plasmonic AgX nanoparticles-modified ZnO nanorod arrays and their visible-light-driven photocatalytic activity. *Chin. J. Catal.* **2014**, *35*, 1113–1125. [CrossRef]

92. Ramasundaram, S.; Seid, M.G.; Choe, J.W.; Kim, E.-J.; Chung, Y.C.; Cho, K.; Lee, C.; Hong, S.W. Highly reusable TiO₂ nanoparticle photocatalyst by direct immobilization on steel mesh via PVDF coating, electrospraying, and thermal fixation. *Chem. Eng. J.* **2016**, *306*, 344–351. [CrossRef]

93. Akerdi, A.G.; Bahrami, S.H.; Arami, M.; Pajootan, E. Photocatalytic discoloration of Acid Red 14 aqueous solution using titania nanoparticles immobilized on graphene oxide fabricated plate. *Chemosphere* **2016**, *159*, 293–299. [CrossRef]

94. Ghoreishian, S.M.; Badii, K.; Norouzi, M.; Malek, K. Effect of cold plasma pre-treatment on photocatalytic activity of 3D fabric loaded with nano-photocatalysts: Response surface methodology. *Appl. Surf. Sci.* **2016**, *365*, 252–262. [CrossRef]

95. Behnajady, M.A.; Moghaddam, S.G.; Modirshahla, N.; Shokri, M. Investigation of the effect of heat attachment method parameters at photocatalytic activity of immobilized ZnO nanoparticles on glass plate. *Desalination* **2009**, *249*, 1371–1376. [CrossRef]

96. Koohestani, H.; Sadrnezhaad, S.K. Photocatalytic Activity of Immobilized Geometries of TiO₂. *J. Mater. Eng. Perform.* **2015**, *24*, 2757–2763. [CrossRef]

97. Hir, Z.A.M.; Moradihamedani, P.; Abdullah, A.H.; Mohamed, M.A. Immobilization of TiO$_2$ into polyethersulfone matrix as hybrid film photocatalyst for effective degradation of methyl orange dye. *Mat. Sci. Semicon. Proc.* **2017**, *57*, 157–165. [CrossRef]

98. Yu, J.; Sun, D.; Wang, T.; Li, F. Fabrication of Ag@AgCl/ZnO submicron wire film catalyst on glass substrate with excellent visible light photocatalytic activity and reusability. *Chem. Eng. J.* **2018**, *334*, 225–236. [CrossRef]

99. Soltani, R.D.C.; Rezaee, A.; Khataee, A.R.; Safari, M. Photocatalytic process by immobilized carbon black/ZnO nanocomposite for dye removal from aqueous medium: Optimization by response surface methodology. *J. Ind. Eng. Chem.* **2014**, *20*, 1861–1868. [CrossRef]

100. Li, C.; Ahmed, T.; Ma, M.; Edvinsson, T.; Zhu, J. A facile approach to ZnO/CdS nanoarrays and their photocatalytic and photoelectrochemical properties. *Appl. Cat. B* **2013**, *138–139*, 175–183. [CrossRef]

101. Sarwar, Z.; Ashraf, M.; Rehman, A.; Aziz, H.; Javid, A.; Nasir, N.; Iqbal, K.; Hussain, T.; Ashar, A. Voltage-assisted photocatalytic activity of ZnO nanorods grown on carbon fabric for effluent treatment. *J. Clean. Prod.* **2018**, *201*, 909–915. [CrossRef]

102. Tang, L.; Jia, C.T.; Xue, Y.C.; Li, L.; Wang, A.Q.; Xu, G.; Liu, N.; Wu, M.H. Fabrication of compressible and recyclable macroscopic g-C3N4/GO aerogel hybrids for visible-light harvesting: A promising strategy for water remediation. *Appl. Cat. B* **2017**, *219*, 241–248. [CrossRef]

103. Li, Y.; Wu, J.; Wu, X.; Suo, H.; Shen, X.; Cui, S. Synthesis of bulk BaTiO$_3$ aerogel and characterization of photocatalytic properties. *J. Solgel Sci. Technol.* **2019**, *90*, 313–322. [CrossRef]

104. Han, H.; Bai, R. Highly effective buoyant photocatalyst prepared with a novel layered-TiO$_2$ configuration on polypropylene fabric and the degradation performance for methyl orange dye under UV-Vis and Vis lights. *Sep. Purif. Technol.* **2010**, *73*, 142–150. [CrossRef]

105. Sannino, D.; Morante, N.; Sacco, O.; Mancuso, A.; De Guglielmo, L.; Di Capua, G.; Femia, N.; Vaiano, V. Visible light-driven degradation of Acid Orange 7 by light modulation techniques. *Photochem. Photobiol. Sci.* **2023**, *22*, 185–193. [CrossRef]

106. Vaiano, V.; Sacco, O.; Libralato, G.; Lofrano, G.; Siciliano, A.; Carraturo, F.; Guida, M.; Carotenuto, M. Degradation of anionic azo dyes in aqueous solution using a continuous flow photocatalytic packed-bed reactor: Influence of water matrix and toxicity evaluation. *J. Environ. Chem. Eng.* **2020**, *8*, 104549. [CrossRef]

107. Mohammed Redha, Z.; Abdulla Yusuf, H.; Amin, R.; Bououdina, M. The study of photocatalytic degradation of a commercial azo reactive dye in a simple design reusable miniaturized reactor with interchangeable TiO$_2$ nanofilm. *Arab J. Basic Appl. Sci.* **2020**, *27*, 287–298. [CrossRef]

108. Alhaji, M.H.; Sanaullah, K.; Khan, A.; Hamza, A.; Muhammad, A.; Ishola, M.S.; Rigit, A.R.H.; Bhawani, S.A. Recent developments in immobilizing titanium dioxide on supports for degradation of organic pollutants in wastewater- A review. *Int. J. Environ. Sci. Technol.* **2017**, *14*, 2039–2052. [CrossRef]

109. Le, A.T.; Le, T.D.H.; Cheong, K.-Y.; Pung, S.-Y. Immobilization of zinc oxide-based photocatalysts for organic pollutant degradation: A review. *J. Environ. Chem. Eng.* **2022**, *10*, 108505. [CrossRef]

110. Magalhães, F.; Moura, F.C.C.; Lago, R.M. TiO$_2$/LDPE composites: A new floating photocatalyst for solar degradation of organic contaminants. *Desalination* **2011**, *276*, 266–271. [CrossRef]

111. Fabiyi, M.E.; Skelton, R.L. Photocatalytic mineralisation of methylene blue using buoyant TiO$_2$-coated polystyrene beads. *J. Photochem. Photobiol. A* **2000**, *132*, 121–128. [CrossRef]

112. Singh, S.; Mahalingam, H.; Singh, P.K. Polymer-supported titanium dioxide photocatalysts for environmental remediation: A review. *Appl. Cat. A* **2013**, *462-463*, 178–195. [CrossRef]

113. Guastaferro, M.; Baldino, L.; Vaiano, V.; Cardea, S.; Reverchon, E. Supercritical Phase Inversion to Produce Photocatalytic Active PVDF-coHFP_TiO$_2$ Composites for the Degradation of Sudan Blue II Dye. *Materials* **2022**, *15*, 8894. [CrossRef]

114. Ata, R.; Sacco, O.; Vaiano, V.; Rizzo, L.; Tore, G.Y.; Sannino, D. Visible light active N-doped TiO$_2$ immobilized on polystyrene as efficient system for wastewater treatment. *J. Photochem. Photobiol. A* **2017**, *348*, 255–262. [CrossRef]

115. Vaiano, V.; Chianese, L.; Rizzo, L.; Iervolino, G. Visible light driven oxidation of arsenite to arsenate in aqueous solution using Cu-doped ZnO supported on polystyrene pellets. *Catal. Today* **2021**, *361*, 69–76. [CrossRef]

116. Vaiano, V.; Matarangolo, M.; Sacco, O. UV-LEDs floating-bed photoreactor for the removal of caffeine and paracetamol using ZnO supported on polystyrene pellets. *Chem. Eng. J.* **2018**, *350*, 703–713. [CrossRef]

117. Sacco, O.; Venditto, V.; Fittipaldi, R.; Vaiano, V.; Daniel, C. Composite polymeric films with photocatalytic properties. *Chem. Eng. Trans.* **2021**, *86*, 571–576. [CrossRef]

118. Daniel, C.; Navarra, W.; Venditto, V.; Sacco, O.; Vaiano, V. Nanoporous polymeric aerogels–based structured photocatalysts for the removal of organic pollutant from water under visible or solar light. In *Visible Light Active Structured Photocatalysts for the Removal of Emerging Contaminants*; Sacco, O., Vaiano, V., Eds.; Elsevier: Amsterdam, The Netherlands, 2020; pp. 99–120. [CrossRef]

119. Sacco, O.; Vaiano, V.; Daniel, C.; Navarra, W.; Venditto, V. Highly Robust and Selective System for Water Pollutants Removal: How to Transform a Traditional Photocatalyst into a Highly Robust and Selective System for Water Pollutants Removal. *Nanomaterials* **2019**, *9*, 1509. [CrossRef] [PubMed]

120. Sacco, O.; Vaiano, V.; Daniel, C.; Navarra, W.; Venditto, V. Removal of phenol in aqueous media by N-doped TiO$_2$ based photocatalytic aerogels. *Mat. Sci. Semicon. Proc.* **2018**, *80*, 104–110. [CrossRef]

121. Vaiano, V.; Sacco, O.; Sannino, D.; Ciambelli, P.; Longo, S.; Venditto, V.; Guerra, G. N-doped TiO$_2$/s-PS aerogels for photocatalytic degradation of organic dyes in wastewater under visible light irradiation. *J. Chem. Technol. Biotechnol.* **2014**, *89*, 1175–1181. [CrossRef]

122. Navarra, W.; Sacco, O.; Daniel, C.; Venditto, V.; Vaiano, V.; Vignati, D.A.L.; Bojic, C.; Libralato, G.; Lofrano, G.; Carotenuto, M. Photocatalytic degradation of atrazine by an N-doped TiO_2/polymer composite: Catalytic efficiency and toxicity evaluation. *J. Environ. Chem. Eng.* **2022**, *10*, 108167. [CrossRef]

123. Mancuso, A.; Vaiano, V.; Antico, P.; Sacco, O.; Venditto, V. Photoreactive polymer composite for selective oxidation of benzene to phenol. *Catal. Today* **2023**, *413–415*, 113914. [CrossRef]

124. Wan, W.; Zhang, R.; Ma, M.; Zhou, Y. Monolithic aerogel photocatalysts: A review. *J. Mater. Chem. A* **2018**, *6*, 754–775. [CrossRef]

125. Hasanpour, M.; Motahari, S.; Jing, D.; Hatami, M. Numerical Modeling for the Photocatalytic Degradation of Methyl Orange from Aqueous Solution using Cellulose/Zinc Oxide Hybrid Aerogel: Comparison with Experimental Data. *Top. Catal.* **2021**, *in press*. [CrossRef]

126. Vaiano, V.; Sacco, O.; Pisano, D.; Sannino, D.; Ciambelli, P. From the design to the development of a continuous fixed bed photoreactor for photocatalytic degradation of organic pollutants in wastewater. *Chem. Eng. Sci.* **2015**, *137*, 152–160. [CrossRef]

127. Chanathaworn, J.; Pornpunyapat, J.; Chungsiriporn, J. Decolorization of dyeing wastewater in continuous photoreactors using TiO_2 coated glass tube media. *Songklanakarin J. Sci. Technol.* **2014**, *36*, 97–105.

128. Dong, G.; Chen, B.; Liu, B.; Hounjet, L.J.; Cao, Y.; Stoyanov, S.R.; Yang, M.; Zhang, B. Advanced oxidation processes in microreactors for water and wastewater treatment: Development, challenges, and opportunities. *Water Res.* **2022**, *211*, 118047. [CrossRef] [PubMed]

129. Das, S.; Srivastava, V.C. Microfluidic-based photocatalytic microreactor for environmental application: A review of fabrication substrates and techniques, and operating parameters. *Photochem. Photobiol. Sci.* **2016**, *15*, 714–730. [CrossRef] [PubMed]

130. Ollis, D.F.; Turchi, C. Heterogeneous photocatalysis for water purification: Contaminant mineralization kinetics and elementary reactor analysis. *Environ. Progress* **1990**, *9*, 229–234. [CrossRef]

131. Knez, Ž.; Markočič, E.; Leitgeb, M.; Primožič, M.; Knez Hrnčič, M.; Škerget, M. Industrial applications of supercritical fluids: A review. *Energy* **2014**, *77*, 235–243. [CrossRef]

132. Reverchon, E.; Schiavo Rappo, E.; Cardea, S. Flexible supercritical CO2-assisted process for poly(methyl methacrylate) structure formation. *Polym. Eng. Sci.* **2006**, *46*, 188–197. [CrossRef]

133. Trucillo, P.; Cardea, S.; Baldino, L.; Reverchon, E. Production of liposomes loaded alginate aerogels using two supercritical CO2 assisted techniques. *J. CO2 Util.* **2020**, *39*, 101161. [CrossRef]

134. Crampon, C.; Boutin, O.; Badens, E. Supercritical Carbon Dioxide Extraction of Molecules of Interest from Microalgae and Seaweeds. *Ind. Eng. Chem. Res.* **2011**, *50*, 8941–8953. [CrossRef]

135. Franco, P.; De Marco, I. Supercritical Antisolvent Process for Pharmaceutical Applications: A Review. *Processes* **2020**, *8*, 938. [CrossRef]

136. Uwineza, P.A.; Waśkiewicz, A. Recent Advances in Supercritical Fluid Extraction of Natural Bioactive Compounds from Natural Plant Materials. *Molecules* **2020**, *25*, 3847. [CrossRef]

137. Okolie, J.A.; Nanda, S.; Dalai, A.K.; Berruti, F.; Kozinski, J.A. A review on subcritical and supercritical water gasification of biogenic, polymeric and petroleum wastes to hydrogen-rich synthesis gas. *Renew. Sustain. Energy Rev.* **2020**, *119*, 109546. [CrossRef]

138. Hu, Y.; Gong, M.; Xing, X.; Wang, H.; Zeng, Y.; Xu, C.C. Supercritical water gasification of biomass model compounds: A review. *Renew. Sustain. Energy Rev.* **2020**, *118*, 109529. [CrossRef]

139. Franco, P.; Pessolano, E.; Belvedere, R.; Petrella, A.; De Marco, I. Supercritical impregnation of mesoglycan into calcium alginate aerogel for wound healing. *J. Supercrit. Fluids* **2020**, *157*, 104711. [CrossRef]

140. Hart, A.; Anumudu, C.; Onyeaka, H.; Miri, T. Application of supercritical fluid carbon dioxide in improving food shelf-life and safety by inactivating spores: A review. *J. Food Sci. Technol.* **2022**, *59*, 417–428. [CrossRef]

141. Wu, H.-T.; Chuang, Y.-H.; Lin, H.-C.; Hu, T.-C.; Tu, Y.-J.; Chien, L.-J. Immediate Release Formulation of Inhaled Beclomethasone Dipropionate-Hydroxypropyl-Beta-Cyclodextrin Composite Particles Produced Using Supercritical Assisted Atomization. *Polymers* **2022**, *14*, 2114. [CrossRef]

142. Dauber, C.; Carreras, T.; González, L.; Gámbaro, A.; Valdés, A.; Ibañez, E.; Vieitez, I. Characterization and incorporation of extracts from olive leaves obtained through maceration and supercritical extraction in Canola oil: Oxidative stability evaluation. *LWT* **2022**, *160*, 113274. [CrossRef]

143. Ozkan, G.; Franco, P.; Capanoglu, E.; De Marco, I. PVP/flavonoid coprecipitation by supercritical antisolvent process. *Chem. Eng. Process.* **2019**, *146*, 1–10. [CrossRef]

144. Franco, P.; Incarnato, L.; De Marco, I. Supercritical CO2 impregnation of α-tocopherol into PET/PP films for active packaging applications. *J. CO2 Util.* **2019**, *34*, 266–273. [CrossRef]

145. Zhang, H.; Wang, C.; Zhang, X.; Zhang, R.; Ding, L. Formation and inhibition of polycyclic aromatic hydrocarbons from the gasification of cyanobacterial biomass in supercritical water. *Chemosphere* **2020**, *253*, 126777. [CrossRef]

146. Chen, Y.; Yi, L.; Wei, W.; Jin, H.; Guo, L. Hydrogen production by sewage sludge gasification in supercritical water with high heating rate batch reactor. *Energy* **2022**, *238*, 121740. [CrossRef]

147. Marrone, P.A.; Hodes, M.; Smith, K.A.; Tester, J.W. Salt precipitation and scale control in supercritical water oxidation—Part B: Commercial/full-scale applications. *J. Supercrit. Fluids* **2004**, *29*, 289–312. [CrossRef]

148. Karmakar, A.; Chandra, A. Water under Supercritical Conditions: Hydrogen Bonds, Polarity, and Vibrational Frequency Fluctuations from Ab Initio Simulations with a Dispersion Corrected Density Functional. *ACS Omega* **2018**, *3*, 3453–3462. [CrossRef] [PubMed]
149. Koech, G.C.; Hatakeda, K. Degradation of reactive dyes by supercritical water oxidation in a batch reactor. *Colour. Technol.* **2002**, *118*, 112–114. [CrossRef]
150. Connolly, J.F. Solubility of Hydrocarbons in Water Near the Critical Solution Temperatures. *J. Chem. Eng. Data* **1966**, *11*, 13–16. [CrossRef]
151. Wang, X.; Gron, L.U.; Klein, M.T.; Brill, T.B. The influence of high-temperature water on the reaction pathways of nitroanilines. *J. Supercrit. Fluids* **1995**, *8*, 236–249. [CrossRef]
152. Kritzer, P.; Dinjus, E. An assessment of supercritical water oxidation (SCWO): Existing problems, possible solutions and new reactor concepts. *Chem. Eng. J.* **2001**, *83*, 207–214. [CrossRef]
153. Baur, S.; Schmidt, H.; Krämer, A.; Gerber, J. The destruction of industrial aqueous waste containing biocides in supercritical water—Development of the SUWOX process for the technical application. *J. Supercrit. Fluids* **2005**, *33*, 149–157. [CrossRef]
154. Jin, F.-M.; Kishita, A.; Moriya, T.; Enomoto, H. Kinetics of oxidation of food wastes with H2O2 in supercritical water. *J. Supercrit. Fluids* **2001**, *19*, 251–262. [CrossRef]
155. Dietrich, M.J.; Randall, T.L.; Canney, P.J. Wet air oxidation of hazardous organics in wastewater. *Environ. Prog.* **1985**, *4*, 171–177. [CrossRef]
156. Mishra, V.S.; Mahajani, V.V.; Joshi, J.B. Wet Air Oxidation. *Ind. Eng. Chem. Res.* **1995**, *34*, 2–48. [CrossRef]
157. Cocero, M.J.; Alonso, E.; Sanz, M.T.; Fdz-Polanco, F. Supercritical water oxidation process under energetically self-sufficient operation. *J. Supercrit. Fluids* **2002**, *24*, 37–46. [CrossRef]
158. Cocero, M.J.; Alonso, E.; Torío, R.; Vallelado, D.; Fdz-Polanco, F. Supercritical Water Oxidation in a Pilot Plant of Nitrogenous Compounds: 2-Propanol Mixtures in the Temperature Range 500−750 °C. *Ind. Eng. Chem. Res.* **2000**, *39*, 3707–3716. [CrossRef]
159. Uygur, A. An overview of oxidative and photooxidative decolorisation treatments of textile waste waters. *J. Soc. Dye. Colour.* **1997**, *113*, 211–217. [CrossRef]
160. Söğüt, O.Ö.; Akgün, M. Removal of C.I. Basic Blue 41 from aqueous solution by supercritical water oxidation in continuous-flow reactor. *J. Ind. Eng. Chem.* **2009**, *15*, 803–808. [CrossRef]
161. Jiang, A.; Cheng, Z.; Shen, Z.; Guo, W. QSAR study on the removal efficiency of organic pollutants in supercritical water based on degradation temperature. *Chem. Cent. J.* **2018**, *12*, 16. [CrossRef]
162. Söğüt, O.Ö.; Akgün, M. Treatment of textile wastewater by SCWO in a tube reactor. *J. Supercrit. Fluids* **2007**, *43*, 106–111. [CrossRef]
163. Söğüt, O.Ö.; Akgün, M. Degradation of aqueous disperse orange 25 by supercritical water oxidation. *Fresenius Environ. Bull.* **2008**, *17*, 864–871.
164. Zhang, J.; Wang, S.; Li, Y.; Lu, J.; Chen, S.; Luo, X. Supercritical water oxidation treatment of textile sludge. *Environ. Technol.* **2017**, *38*, 1949–1960. [CrossRef]
165. Li, J.; Wang, S.; Jiang, Z.; Yang, C.; Xu, H. Supercritical water oxidation of dyeing sludge. *IOP Conf. Series Earth Environ. Sci.* **2019**, *233*, 052004. [CrossRef]
166. Söğüt, O.O.; Akgün, M. Treatment of dyehouse waste-water by supercritical water oxidation: A case study. *J. Chem. Technol. Biotechnol.* **2010**, *85*, 640–647. [CrossRef]
167. Wang, Q.; Lv, Y.; Zhang, R.; Bi, J. Decomposition of dyeing wastewater by supercritical water oxidation. *Fresenius Environ. Bull.* **2013**, *22*, 3588–3595.
168. McCarthy, B.J. Biotechnology and coloration. *Colour. Technol.* **1997**, *27*, 26–31. [CrossRef]
169. Crooker, P.J.; Ahluwalia, K.S.; Fan, Z.; Prince, J. Operating Results from Supercritical Water Oxidation Plants. *Ind. Eng. Chem. Res.* **2000**, *39*, 4865–4870. [CrossRef]
170. Yang, B.; Shen, Z.; Cheng, Z.; Ji, W. Total nitrogen removal, products and molecular characteristics of 14 N-containing compounds in supercritical water oxidation. *Chemosphere* **2017**, *188*, 642–649. [CrossRef] [PubMed]
171. Yang, B.; Cheng, Z.; Tang, Q.; Shen, Z. Nitrogen transformation of 41 organic compounds during SCWO: A study on TN degradation rate, N-containing species distribution and molecular characteristics. *Water Res.* **2018**, *140*, 167–180. [CrossRef]
172. Aymonier, C.; Beslin, P.; Jolivalt, C.; Cansell, F. Hydrothermal oxidation of a nitrogen-containing compound: The fenuron. *J. Supercrit. Fluids* **2000**, *17*, 45–54. [CrossRef]
173. Li, H.; Oshima, Y. Elementary Reaction Mechanism of Methylamine Oxidation in Supercritical Water. *Ind. Eng. Chem. Res.* **2005**, *44*, 8756–8764. [CrossRef]
174. Bermejo, M.D.; Fdez-Polanco, F.; Cocero, M.J. Effect of the Transpiring Wall on the Behavior of a Supercritical Water Oxidation Reactor: Modeling and Experimental Results. *Ind. Eng. Chem. Res.* **2006**, *45*, 3438–3446. [CrossRef]